Orthogonal degron system for controlled protein degradation in cyanobacteria

Jonathan K. Sakkos¹, Sergio Hernandez-Ortiz², Katherine W. Osteryoung³, Daniel C. Ducat^{1,4,*}

- ¹ MSU-DOE Plant Research Laboratory, Michigan State University, East Lansing, MI 48824, USA
- ² Department of Microbiology & Molecular Genetics, Michigan State University, East Lansing, MI 48824, USA
- ³ Department of Plant Biology, Michigan State University, East Lansing, MI 48824, USA
- ⁴ Department of Biochemistry & Molecular Biology, Michigan State University, East Lansing, MI 48824, USA
- * Corresponding author: email ducatdan@msu.edu, phone (517) 432-5118

ABSTRACT

Synechococcus elongatus PCC 7942 is a model cyanobacterium for study of the circadian clock, photosynthesis, and bioproduction of chemicals, yet nearly 40% of its gene identities and functions remain unknown, in part due to limitations of the existing genetic toolkit. While classical techniques for the study of genes (e.g., deletion or mutagenesis) can yield valuable information about the absence of a gene and its associated protein, there are limits to these approaches, particularly in the study of essential genes. Herein, we developed a tool for inducible degradation of target proteins in *S. elongatus* by adapting a method using degron tags from the *Mesoplasma florum* transfer-messenger RNA (tmRNA) system. We observed that *M. florum* lon protease can rapidly degrade exogenous and native proteins tagged with the cognate sequence within hours of induction. We used this system to inducibly degrade the essential cell division factor, FtsZ, as well as shell protein components of the carboxysome. Our results have implications for carboxysome biogenesis and the rate of carboxysome turnover during cell growth. Lon protease control of proteins offers an alternative approach for the study of essential proteins and protein dynamics in cyanobacteria.

INTRODUCTION

Cyanobacteria are prokaryotic microbes that convert CO₂ and sunlight into stored energy and organic carbon via oxygenic photosynthesis. The relative simplicity of these photoautotrophic microbes and their genetic tractability has made them useful subjects for fundamental science and application-driven research. One such organism, *Synechococcus elongatus* PCC 7942 (hereafter *S. elongatus*), is a model for studying photosynthesis^{1–6}, the circadian clock ^{7–9}, carbon concentrating mechanisms ^{10–14}, and a platform for bioproduction of chemicals ^{15–19}. While many efforts are ongoing to improve the fundamental understanding of *S. elongatus* in these research areas, there remains much to be learned about its genome, as approximately 40% of gene functions are unknown and 26% of its genes are essential (>700

genes of 2,723 total in the genome)²⁰. Furthermore, biotechnological applications could benefit from increased refinement of the cyanobacterial genetic toolkit.

Despite considerable interest in cyanobacteria as bioproduction crop species, the molecular biology toolkit of genetic parts is lacking in comparison with other heterotrophic workhorse species, such as *Escherichia coli*, *Saccharomyces cerevisiae*, *and Bacillus subtilis* ²¹. Several classical techniques (*e.g.*, gene deletion, mutagenesis, transposon insertion) are routinely used to modify genes in the genome or control transcript levels, each of which have attendant strengths and limitations. For instance, gene deletion is widely used to study protein function, but it cannot be used for essential proteins by definition and knockout phenotypes are frequently complicated by compensatory mutations that arise elsewhere in the genome²². Transposable elements and site-directed mutagenesis are useful in generating genomewide mutant libraries and gene-specific mutations, respectively, but both alter the gene product(s) and disrupt gene regulation, which convolutes functional analysis^{23–25}. RNA and CRISPR interference (RNAi, CRISPRi) have been recently adapted to some cyanobacterial models allowing sequence-specific repression of target genes, but these methods may be toxic to host cells and require a large degree of optimization, while still having variable success rates ^{26–29}.

Techniques that enable protein-level control provide a complementary approach for gene functional studies that can circumvent some aforementioned technical shortcomings³⁰. Directly targeting the protein of interest does not disturb transcriptional or translational processes, thus preserving genetic regulatory elements. The transfer-messenger RNA (tmRNA) ribosome rescue system natively appends a C-terminal ssrA peptide (degron) onto nascent, aberrant peptides originating from damaged mRNA in a stalled ribosome, which targets the peptide for rapid proteolysis^{31–33}. Studies have made use of this system by inserting the ssrA sequence directly onto gene targets, greatly reducing the stability of the protein product of the modified gene. Appending ssrA tags has been shown to modulate steady-state protein level in *Synechocystis sp.* ³⁴, while in *E. coli* native degrons have also been used in genetic oscillatory clocks and to enable control over the degradation rate of tagged proteins ³⁵. Protein quality control is a conserved process in prokaryotes with little variance in degron sequences³⁶, and ssrA degron tag sequences may differ by only a limited number of residues (e.g., key C-terminal amino acid residues for recognition between the distant species *E. coli* and *S. elongatus* are LAA vs. VAA, respectively^{32,37,38}).

Orthogonal control of protein stability requires a sufficiently different degron sequence and cognate protease to ensure the foreign degron is a poor target for native proteolytic machinery and to limit targeting of native proteins by the heterologous protease. The protein quality control system of *Mycoplasma* species utilizes a single cytoplasmic protease, the Lon protease, whose degron length and sequence recognition has diverged significantly³⁶. Based on the uniqueness of the Lon protease of *Mesoplasma florum (mf-lon, M. florum)*³⁹, a recent study developed a novel tool in *E. coli* to destabilize degron-tagged proteins upon heterologous expression of *mf-lon* ³⁶. This system can be made to be tunable and inducible if *mf-lon* is placed under an appropriate promoter, allowing protein loss to be followed in real time. Furthermore, protein degradation systems can be utilized to construct more complex

genetic circuits, including toggle switches, oscillators, containment systems, and dynamic control of metabolic flux ^{40–43}.

We sought investigate the efficacy of *mf-lon* for controlling target protein stability in *S. elongatus*, which has not been previously reported. *S. elongatus* has limited alternative methods for regulating protein, though CRISPRi has recently shown promise in cyanobacteria ^{28,44}. The real-time downregulation of proteins of interest can also enable a different approach for the study of dynamic processes in cyanobacteria. In this work, we report successful integration of *mf-lon* protease, and optimize conditions to precisely regulate the stability of target proteins while minimizing off-target effects.

RESULTS

Construction and validation of inducible mf-lon S. elongatus strains

We first designed and integrated mf-lon to be heterologously expressed in S. elongatus under a theophylline-dependent riboswitch (Figure 1). To conduct a preliminary characterization of the mf-lon system in S. elongatus, we built an IPTG-inducible fluorescent protein reporter (mNeonGreen; mNG) which encoded a C-terminal degron fusion. The theophylline-dependent riboswitch 52 enabled inducible control of the mf-lon protease independently of the mNG-PDT reporter, although both constructs were driven by the strong promoter P_{trc} (Figure 2A). Cytosolic mNG-PDT was abundant in the absence of mflon expression (Figure 2B) but was significantly attenuated after theophylline was added (Figure 2C). Flow cytometry was used to quantitatively measure the reporter fluorescence in cell populations 24 hours after mf-lon expression and the normalized fluorescence intensity was reduced to 14.93 ± 2.19 % of the uninduced controls, a ~7-fold reduction in reporter protein abundance in the ON vs OFF state (Figure 2D). All cells of the theophylline-treated population exhibited a reduction in reporter fluorescence at 24 hours and the degree of reduction was positively correlated to the theophylline concentration (Figure S1), as was the accumulation of mf-lon (Figure S2). We tracked the kinetics of mf-lon-mediated proteolysis of the reporter immediately following *mf-lon* expression as a function of inducer concentration and observed that the initial rate of fluorescence loss was dependent on the titration of theophylline inducer (Figure 2E). Near complete degradation of mNG-PDT occurred in less than 24 hours with 10-30 µM theophylline, with 50% protein knockdown in less than 3 hours. More rapid knockdown of the reporter (~90% in two hours) was seen with high mf-lon induction (1 mM theophylline, S3). We also varied the level of mNG-PDT substrate by titrating the IPTG concentration (Figure 2F; red line) and observed that mf-lon expression (30 µM theophylline) was sufficient to repress fluorescence of the reporter at any induction level (Figure **2F**; blue line). This suggests that the available *mf-lon* protease at 30 μM theophylline was sufficient to degrade the mNG-PDT target under these conditions (Figure 2F). The dynamic range of reporter abundance between the ON/OFF states of mf-lon was proportional to the concentration of mNG in the absence of mf-lon (Figure 2G).

High expression of Lon Protease results in off-target proteolysis

Ideally, mf-lon protease should specifically recognize its cognate degron and be orthogonal to native proteolytic machinery in S. elongatus; therefore, we examined the fidelity of this system. There was a negligible difference in the fluorescence of an untagged mNG reporter when mf-lon was expressed (1 mM theophylline), suggesting that mf-lon does not appreciably degrade mNG without a cognate PDT sequence (Figure 3A, left panel). However, there appeared to be some recognition of the mf-lon PDT by native proteolytic machinery in S. elongatus, as evidenced by the significantly lower basal expression level of a mNG-PDT reporter relative to the untagged mNG control, even when the strain background did not encode mf-lon (Figure 3A, right panel). Furthermore, genomic integration of mf-lon reduced the normalized reporter fluorescence of mNG-PDT by an additional 15%, even without protease induction (Figure 3A, +mf-lon), which might be due to leaky expression of mf-lon in the absence of inducer. In an attempt to reduce the recognition of the degron by native proteolytic machinery, we performed sitedirected mutagenesis on the first four PDT residues (i.e., AANK), which showed partial homology to the S. elongatus ssrA sequence. Preliminary results in a WT background suggested that these mutations might slightly improve the stability of the tagged reporter protein (Figure S3). However, the improvement in basal reporter abundance by mutating these residues was negligible in a background with genomic integration of *mf-lon* (**Figure S4**). Therefore, we proceeded with characterization of the original PDT sequence.

When *mf-lon* was induced at higher levels (1 mM theophylline) we observed indications that this protease could destabilize off-target, endogenous proteins. First, cells exhibited a strong growth arrest under this level of *mf-lon* expression, though slower growth than wild type was observed in all *mf-lon* containing cell lines (**Figure S5**). To identify possible native proteins that might be off-target substrates for *mf-lon*, we over-expressed *mf-lon* at the higher inducer concentration (1 mM theophylline) and conducted a proteomics analysis in the hours immediately following. We detected 1147 total cellular proteins as part of our analysis, the majority of which were not significantly affected by *mf-lon* expression. However, 42 proteins exhibited statistical downregulation (Kruskal-Wallis Test: p < 0.05, Benjamini-Hochberg: p < 0.00187 (highlighted in green), **Supplemental Spreadsheet**) and these genes were enriched for components of the photosynthetic machinery and ribosomes (**Figure 3B**). Of the 42 most statistically significant genes identified, 12 were linked to the phycobilisome, 6 to Photosystem I, and 4 to ribosomal processes (**Figure 3C**). Bioinformatic analysis of the sequence of downregulated proteins did not uncover any obvious shared features or cryptic sequences that resemble the *mf-lon* degron tag^{36,50,62}.

Since proteins related to photosynthesis were preferentially affected by off-target proteolysis, we optimized *mf-lon* induction using photosynthetic parameter measurements as a sensitive indicator of unintended impacts on the cell. We hypothesized that off-target effects might be mitigated by titrating the abundance of *mf-lon*, and therefore determined if limiting excess protease abundance for reporter

degradation reduced unintended proteolysis. As expected from the aforementioned growth arrest phenotype and proteomics data, at high *mf-lon* induction (1 mM theophylline), photochemical quenching (q_P) and the quantum yield of Photosystem II (Φ_{II}) were severely impaired (**Figure 3D**). However, at theophylline concentrations <40 µM, there were no statistical differences in q_P and Φ_{II} between treatments. Thus, by limiting *mf-lon* induction conditions to 30 µM or less theophylline, undesired proteolysis was diminished while efficient degradation of PDT-tagged proteins could still be achieved (**Figure 2**).

Native protein tagging permits real-time inactivation of essential proteins

We next examined the downregulation of endogenous *S. elongatus* protein targets by *mf-lon*, focusing on the control of essential proteins. We targeted FtsZ, an essential protein that forms homopolymeric filaments that guide septum formation and contraction and are required for cell division ^{69–71}. Impaired FtsZ function is known to lead to dramatically increased cell length, providing a useful diagnostic phenotype (**Figure S6A**) ^{56,72,73}. Strains we initially generated in a WT background where the endogenous *ftsZ* locus was modified to encode a full-length PDT at the C-terminus did not appear to elongate appreciably; whereas with the genomic integration of *mf-lon*, cells were highly elongated even in the absence of *mf-lon* induction (**Figure S7**). This suggested that some pathways may be more sensitive to modest changes in protein stability and might require the use of a PDT with a lower affinity to proteolytic machinery (both native and exogenous).

Prior reports have characterized PDT variants with lowered *mf-lon* affinity, including an abbreviated PDT with the first 13 residues removed ^{58,74}, thus we altered the tag on FtsZ to this truncated form (FtsZ-PDT*). *S. elongatus* cells where the endogenous copy of *ftsZ* was fused to the truncated PDT were similar in length to WT cells in the absence of theophylline, but reproduced the previously reported elongation phenotype ^{72,73} upon induction of *mf-lon* (**Figure 4B**). Measurement of cell length in the hours immediately following *mf-lon* induction revealed that they elongated constantly (**Figure 4C**) at a rate of ~0.89 μm/hour (R² = 0.998). This rate of elongation was observed even at the earliest time point measured (4 hours post theophylline addition), suggesting that the division arrest phenotype initiated almost immediately after *mf-lon* induction. Similarly, while intact FtsZ rings positioned at the cell midpoint were observed by immunofluorescence in FtsZ-PDT* lines, FtsZ staining was diminished and disorganized in cells within 4 hours of *mf-lon* expression (**Figure 4D**).

To test whether the elongation phenotype could be reversed, we treated cells with theophylline for 24 hours, then removed the inducer and imaged the cells after a 24 hour recovery period. We observed that cell division was restored, with asymmetric daughter cells ⁷⁵ budding from the ends of elongated mother cells (**Figure 4E**). The control cells not exposed to theophylline did not change in length (**Figure S8A**),

while the cells with continued theophylline induction through the recovery period remained elongated (Figure S8B).

Proteins within complexes and assemblies can be targeted by mf-lon

Because protein-level targeting approaches downregulate factors in real time, they might be used to elucidate dynamic protein functions that would be difficult to ascertain with a gene knockout. Using the *mf-lon* system, the transition from the native state to knockout-like conditions can be observed. This may be particularly valuable for multi-subunit protein complexes, where the function of the whole assembly is interdependent with the functioning of multiple proteins. One such complex is the cyanobacterial carboxysome, a proteinaceous, selectively permeable bacterial microcompartment (BMC) that facilitates Rubisco's carboxylation activity under atmospheric CO₂ ⁷⁶. Shell proteins (e.g., CcmK2, CcmO, CcmL) encapsulate cargo enzymes responsible for carbon fixation (**Figure 5A**) ^{77,78}. To validate the use of *mf-lon* on protein complexes, we generated separate strains with C-terminal degron fusions to the endogenous *ccmO* and *ccmL* genes. Both of these shell proteins are required for carboxysome integrity, and knockout of these genes leads to distinguishable defects in carboxysome morphology ^{10,79,80}. We therefore also integrated a fluorescent reporter fused to the small subunit of Rubisco (RbcS-mNG), to allow visualization of changes in carboxysome organization (**Figure 5A**, **S6A**, **S9**).

Mutant strains with the genomic copies of ccmO or ccmL tagged with a PDT exhibited normal carboxysome morphology and positioning in the absence of *mf-lon* expression (**Figures 5**, **S9**), but displayed reorganized carboxysomes following *mf-lon* induction. CcmO-PDT mutants where *mf-lon* was induced (30 μM theophylline), exhibited atypical carboxysome morphology and the formation of large polar bodies containing the RbcS reporter (**Figure 5B**). This phenotype is highly reminiscent of prior reports of carboxysome organization in Δ*ccmO* mutants ^{10,79,80}. Although this phenotype was not fully penetrant, quantitative analysis of the RbcS-mNG reporter found that Rubisco accumulated into fewer and larger aggregates as represented by the distribution of foci per unit cell length, which shifted from a mean of 1.41 ± 0.29 foci/μm to 0.51 ± 0.24 foci/μm (**Figure 5C**). Averaging the positioning of reporter fluorescence across many cells (n>2000) illustrated the strong concentration of Rubisco to cell poles when *mf-lon* was induced and CcmO-PDT was degraded (**Figure 5D**). By comparison, *mf-lon* induction in CcmL-PDT mutant background led to a reduction in the number of foci per unit length, concentration of RbcS-mNG along the center of the cells, and the formation of elongated, rod-shaped carboxysomes (**Figure S10**). This rod phenotype is well-established for Δ*ccmL* mutants but is not typical in mutants lacking *ccmO* ¹⁰.

We used *mf-lon* to investigate temporal changes in Rubisco distribution with a degron-tagged CcmO. Within 24 hours after *mf-lon* induction, we qualitatively observed increased heterogeneity in foci intensity and foci aggregation (**Figure 6A**). In these early stages, intermediate phenotypes were observed relative to the more obvious polar Rubisco aggregation observed later. These included a gradual mispositioning of carboxysomes (**Figure 6B**), decreased carboxysome number per unit cell length (**Figure 6C**), and

increasing inter-carboxysome spacing (Figure 6D). These trends continued to progress over time (72 hours; Figure S11), possibly indicating loss of productive interaction with the carboxysome positioning machinery⁸¹ as the carboxysome shell integrity became increasingly compromised. Qualitatively, we observed an increase in the heterogeneity of RbcS-mNG intensity between different carboxysomes within the same cell following downregulation of CcmO-PDT (Figures 6, S11), possibly suggesting clustering/fusion of multiple carboxysomes over time. The overall integrated fluorescence signal of RbcSmNG within mf-lon expressing cells remained similar to that of uninduced controls, suggesting RbcSmNG levels did not change significantly, but that the RbcS-mNG reporter was instead reorganized after CcmO downregulation (Figure 6B, E). Interestingly, induction of *mf-lon* lowered the background reporter intensity in the cytosol nearly 30%, while foci intensity increased (Figure 6A, E, , S13), potentially representing a recruitment of cytosolic Rubisco to one or more compromised carboxysomes even early on, while the dominant $\Delta ccmO$ phenotype was not evident. Because some of the intermediate phenotypes we observed were more subtle and less penetrant, we display a randomized representative sampling of RbcS-mNG fluorescence during a time-series of CcmO degradation in , S12. These images show qualitative trends of deterioration in carboxysome organization. In all measured cases, the total fluorescence signal of RbcS-mNG per cell was invariant relative to controls where mf-lon was not induced.

DISCUSSION

In this work, we developed a tool to inducibly degrade proteins of interest in *S. elongatus* by a C-terminal fusion of degron tags from the *M. florum* tmRNA system ³⁹. To our knowledge, this is the first report using *mf-lon* in cyanobacteria. We showed that target proteins can be rapidly degraded in as little as 2 hours following heterologous expression of *mf-lon*, though lower induction of *mf-lon* can tune down the rate of degradation. We demonstrated that this tool can be used to study the function of essential proteins, such as the cell-division protein FtsZ, and to examine dynamics of proteins that are part of larger complexes (e.g., components of the carboxysome). This tool offers an alternative approach for the study of essential proteins, protein dynamics, and applied molecular engineering in cyanobacteria – though we also identified limitations that must be taken into consideration for the effective use of this approach.

Off-target effects can be mitigated by titration of *mf-lon* induction

While the idealized *mf-lon* protein degradation system would be a completely orthogonal pathway to native proteolytic machinery, we found evidence for off-target proteolysis and degron recognition by endogenous proteases. When *mf-lon* was strongly expressed (1 mM theophylline) in *S. elongatus*, we observed a severe impairment of photosynthetic processes and a growth arrest, likely caused by off-target degradation of endogenous proteins (**Figures 3, S4**). The most strongly downregulated off-target

proteins following over-expression of *mf-lon* were associated with photosynthesis (**Figure 3B, C**). Among the most strongly impacted cell features were the phycobilisomes, where we observed that 8 proteins (of 16 total phycobilisome subunits encoded in *S. elongatus*) were significantly downregulated at 2-4 hours after induction of *mf-lon*.

The observation that high expression of *mf-lon* leads to off-target protein downregulation of endogenous factors stands in contrast with the results of Cameron and Collins ³⁹, who did not report similar effects in *E. coli* or *Lactobacillus lactis*. Furthermore, the concentration of off-target effects on photosynthesis-related proteins (**Figure 3B, C**) is unfortunate given that cyanobacteria are specifically targets of bioindustrial interest due to their potential for capturing solar energy ^{82,83}. On the other hand, since chlorophyll *a* fluorescence measurements provide a non-invasive read-out of photosynthetic performance that is fairly sensitive to even minor changes in the abundance of photosynthetic proteins ⁸⁴, such measurements can also be used to screen for conditions where the off-target impacts of mf-lon are minimized (**Figure 3D**). It is noteworthy that inducing *mf-lon* at levels that minimized off-target effects (≤30 µM theophylline) also slowed the kinetics of fluorescent reporter proteolysis compared to strong induction (~1 mM, **Figure S3, 2E**); although the negative impacts of a strong *mf-lon* induction are likely to outweigh the faster degradation rate of protein targets for most applications.

In addition, we found evidence that the PDT tags were partially recognized by native proteolytic machinery, despite limited sequence similarity to the *S. elongatus* ssrA tag (*se-ssrA*). (**Figure 3A**). It is possible that *S. elongatus* possesses adaptor proteins that may recognize *mf*-PDT, analogous to the SspB protein in *E. coli*, which targets ssrA-tagged peptides to ClpXP by binding residues 1-4 and 7 (AAND-Y) of the *ec-ssrA* ^{37,85}. Indeed, though there is no known SspB homolog in *S. elongatus*, site-directed mutagenesis of residues 1-4 of the PDT used in this study could improve the basal reporter stability by 75-350% (**Figure S4**). Since the full 27 amino acid sequence is not required for proteolysis ^{58,74}, further optimization of the *mf-lon* degron by systematic deletion of problematic residues could improve fidelity of the system ⁸⁶. In addition, tightening unwanted *mf-lon* expression with additional repression, or transcriptional isolators might enhance the dynamic range of this platform ^{52,57,87–89}.

Essential proteins in cyanobacteria can be studied with *mf-lon*

As a proof-of-principle example that mf-lon could be used to control stability of essential proteins, we targeted FtsZ, a critical component of the cell division machinery. Strains where the endogenous ftsZ gene was fused with a PDT (FtsZ-PDT*) reproduced the well-established cell elongation phenotype when mf-lon was expressed (**Figures 4B, S6A**) 72,73 . Relative to the normal elongation rate of S. elongatus in exponential phase (i.e., \sim 0.75 μ m/hour: 8-hour doubling, dividing cell length of \sim 6 μ m), we observed a population level elongation rate of 0.89 μ m/hour in the first hours immediately following mf-lon induction. This suggests that cytosolic FtsZ-PDT* is almost instantaneously (within minutes) reduced to a level insufficient for division. This observation stands in contrast to other proteins we investigated that were not

downregulated so rapidly. It is likely that lower basal abundance, more rapid turnover, and/or cooperative effects of FtsZ subunits could contribute to this rapid phenotypic onset ^{90–93}.

In comparison to other methods for protein downregulation in cyanobacteria, *mf-lon* appears to control protein level more rapidly. Zhang *et al.* used RNA-based gene repression to study proteins involved in cell morphology (*e.g.*, FtsZ, MreB, and ZipN), but significant changes in cell length were not present until 2-5 days after induction ⁹⁴. Similarly, Yao *et al.* observed maximal CRISPRi repression of 94% in a fluorescent reporter after 4 days of induction ²⁸. Taton and coworkers developed a NOT gate, a type of genetic logic gate that represses expression upon activation of the gate ⁹⁵, which was able to achieve over 90% downregulation in 2-4 days in *S. elongatus*, but this system cannot be used to target genes in their native context, due to how the circuit was constructed ⁹⁶. *Mf-lon* induction led to an 86% decrease in reporter fluorescence within 24 hours (**Figure 2D, E**), and the appearance of expected phenotypic changes within hours of engagement (**Figures 4, 6**).

Targeting protein complexes with mf-lon

The rapid onset of protein degradation has the potential advantage of allowing "real-time" visualization of cellular effects immediately following protein loss, including proteins that are subunits of larger complexes. The carboxysome has been the subject of several recent works investigating *in vivo* assembly mechanisms, including CcmM-mediated organization of Rubisco via liquid-liquid phase separation (LLPS) and shell encapsulation of cargo proteins via CcmM and CcmN ^{97–99}. Such studies established carboxysome-associated gene deletion phenotypes, and validated use of fluorescent carboxysome reporters (e.g., fluorescent fusions of RbcS, RbcL, or CcmK2) ^{10,79,80}.

We found that *mf-lon*-mediated downregulation of two selected shell proteins, CcmO and CcmL, replicated the distinct closure defects found in knockout mutants of these same genes 10,79,80 . CcmO is a shell protein of unknown structure $^{76-78}$, with knockout mutants ($\Delta ccmO$) that accumulate aggregated shell and cargo proteins at the cell pole, and where integrity of the shell is compromised, as demonstrated by incapacity of growth under atmospheric CO_2 10,79,80 . CcmL is a pentamer (BMC-P) made of a single Pfam03319 domain which caps the vertices of the icosahedral BMC shell 76,77 . Mutants lacking CcmL ($\Delta ccmL$) are unable to close the carboxysome shell and form rod-like carboxysomes 10 . We find that specific targeting of PDT-tagged subcomponents of the larger complex shell was possible, as evidenced by the reproduced phenotypes of $\Delta ccmO$, consisting of polar Rubisco aggregates (**Figure 5**), and $\Delta ccmL$ -specific phenotype of elongated rod-like carboxysomes (**Figure S9**) following their respective degradation.

The dynamics of carboxysome shell defect phenotypes caused by targeted proteolysis has implications for the natural functioning of these microcompartments. For example, we observed the onset of severe carboxysome phenotypes 8-24 hours after *mf-lon* expression. When compared with the mNG reporter degradation rate (<24 hours to maximal downregulation; **Figure 2E**), or the occurrence of cell

elongation following FtsZ degradation (<1 hour; Figure 4), carboxysome phenotypes took up to 3 days to reach maximal penetrance (Figure 5/6). One possibility is that the PDT tags were inefficiently targeted for shell proteins, though both structural studies of purified carboxysome shells, and homology models indicate that the C-termini of both CcmO and CcmL should face the cytosol while they are integrated into the shell 100. Regardless, if steric clash contributes to a reduced efficiency of *mf-lon* recognition, the relatively slow rate of phenotype onset would be indicative of a slow rate of shell protein dissociation from the oligomeric form encapsulating the cargo to a soluble form. Quantification of this in more targeted studies could have implications for our understanding of how dynamic the carboxysome is once it has been fully assembled, which is an outstanding question in the field of carboxysomes and related BMCs. Another outstanding question relates to the dominant mechanism and origin of carboxysome biogenesis. It is currently unresolved if the majority of new carboxysomes form at the cell pole, first as procarboxysomes which are encapsulated and spatially segregated ¹⁰, or as the result of fission from existing carboxysomes 11. In contrast to the phenotypes observed many hours after CcmO-PDT degradation (which resembled established knockout phenotypes), we observe evidence that would be consistent with recruitment of a cytosolic Rubisco pool to a subset of carboxysomes (Figure 5D, 6B/E). This observation has at least two components with potential implications for carboxysome biogenesis; i) there is a substantial cytosolic pool of RbcS which is significant enough to visualize and track, but which is not aggregated within the cytosol, and ii) the cytosolic RbcS is capable of binding to existing carboxysome luminal components but may be sequestered until the carboxysome shell becomes compromised (Figures 5, S12, S13). One implication is that the cytosol under these growth conditions may be relatively limited for Rubisco aggregating factors (e.g., short or long CcmM isoforms), as we do not see aggregates outside of the carboxysomes despite a significant fraction of RbcS-mNG in the cytosol. Following CcmO degradation, the recruitment of this RbcS-mNG pool to carboxysomes, may resemble the fission-based biogenesis model as proposed by Chen and coworkers¹¹. Indeed, a recent study by Hill et al. hypothesized that shell breakage may be a rate-limiting step regulating carboxysome turnover and fate 101. In the context of this discussion, it is important to note that there is a separate pool of endogenous (untagged) RbcS that we cannot assess by microscopy which could behave differently from RbcS-mNG. The *mf-lon* system may be optimally suited to controllably degrade shell proteins, remove proteolytic activity, and interrogate whether carboxysome degradation is inevitable once the complex becomes sufficiently damaged or whether remodelling and repair can occur.

Potential opportunities for study with a targeted protein degradation system

Targeted proteolysis with *mf-lon* can be a useful tool for the fundamental study of protein function and molecular engineering in cyanobacteria beyond the examples in this work. By focusing on one protein at a time and observing the emergent phenotypes after proteolytic downregulation, multicomponent protein complexes can be dissected in a systematic, controllable way to gain additional insight into their

functions. Both the cyanobacterial carboxysome and photosynthetic machinery are apt targets due to their respective complexities and lack of complete understanding of their biogenesis. Particularly in cases where gene deletion causes compensatory mutations or dynamic interplay between proteins, precise and real-time targeting may have advantages over existing techniques ²². Proteins associated with cell division (e.g., ZipA, FtsZ, Ftn2), and stress response (e.g., RpaB, NbIA) are also examples of potential targets for pulse-chase knockdown with *mf-lon*. There is also significant interest in sustainable bioproduction with cyanobacterial chassis and using *mf-lon* to actively reroute carbon flux has the potential to improve yield and allow fine-tuned control of metabolic pathways for system optimization ^{27,83,102,103}. Furthermore, *mf-lon* is not limited to targeting a single protein at a time. Multiple proteins can be tagged with a degron without additional modifications, allowing simultaneous knockdown. Finally, while partial knockout of essential genes in cyanobacteria can be achieved, it is often hampered by insufficient penetrance. The use of *mf-lon* in conjunction with a gene deletion meroploid may be one way to achieve a near-knockout.

METHODS

Microbial culturing conditions

S. elongatus cultures (50-100 mL) were grown in baffled flasks (Corning) with BG-11 medium (Sigma) supplemented with 1 g/L HEPES, pH 8.3, in a Multitron II shaking incubator (Infors HT). Cultures were grown under continuous light with GroLux bulbs (Sylvania) at 125 µmol photons m⁻² s⁻¹, 2% CO₂, 32°C, and with 130 rpm shaking. Prior to all experiments, cultures were back-diluted daily into antibiotic-free medium for ≥3 days to ensure all experiments were conducted with cultures during exponential growth. When antibiotics were used for selection purposes, they were supplemented at 12.5 µg/mL for kanamycin, 25 µg/mL spectinomycin, or 25 µg/mL chloramphenicol.

Genetic assembly and strain transformation

Genetic constructs were generated using Isothermal Assembly from either PCR-amplified or synthesized dsDNA (Integrated DNA Technologies) ⁴⁵. Constructions for integration of DNA in cyanobacterial genome were flanked with 300-500 bp of homology to promote efficient recombination ⁴⁶. Chemically competent *E. coli* DH5α were prepared and transformed as is routine ^{47–49}. *S. elongatus* cells were transformed as previously described ^{50,51}. All constructs were confirmed by PCR and Sanger sequencing. See **Table 1** for plasmids used in this study. A list of *S. elongatus* strains used in this study can be found in **Table 2**.

Protein degradation tag and derivations

Unless otherwise noted, the base protein degradation tag (PDT) sequence "AANKNEENTNEVPTFMLNAGQANRRRV" was used, which is identical to PDT #3 reported in Cameron

& Collins, 2014. Initial characterization of the fluorescent reporter was conducted using the mNeonGreen sequence ⁵³, with a C-terminally appended PDT tag (mNG-PDT). These constructs were integrated at Neutral Site 3 (NS4; ⁵⁴) under the control of a Ptrc promoter (IPTG inducible). Reporter strains were induced with 1 mM IPTG for 48-72 hours prior to mf-lon induction with daily back-dilution. A theophyllinedependent riboswitch that was previously developed 52 and which has been demonstrated to provide tunable control in a variety of applications in *S. elongatus* ^{15,55–57} was used to control *mf-lon* expression. Unless otherwise noted, mf-lon was induced with 30 µM theophylline. Modification of the PDT was performed using two methods for site-directed mutagenesis. In the native recognition screening mutants, the first four residues (AANK) were independently changed to aspartic acid 58 59 via a modified version of the QuickChange method (Zheng et al., 2004). Briefly, primers were designed with ~30 bp of homology centered on the target site and ~8 bp 3' overhangs using PrimerX (http://bioinformatics.org/primerx). A silent mutation was inserted downstream of the target site to create a BseRI restriction site to facilitate rapid selection of properly modified plasmids using WatCut (http://watcut.uwaterloo.ca/) via primer pairs amplifying plasmid backbone #848 (see Table 1). PDT truncation to retain residues 14-27 (TFMLNAGQANRRRV) was done via inverse PCR to excise the PDT, followed by Gibson Assembly, with annealed primers containing the desired sequence and homology regions.

Microscopy & Image Analysis

All live-cell microscopy was performed on cells in exponential growth by centrifuging 2 mL of culture at 5,000 × g for 5 minutes, resuspending into 100-200 µL of BG-11, and transferring a 2 µL aliquot to a 3% agarose pad. The cells were allowed to briefly equilibrate (≥10 minutes) before the pad was placed onto a #1.5 glass coverslip for imaging. Images were captured using a Zeiss Axio Observer D1 inverted microscope equipped with an Axiocam 503 mono camera and a Zeiss Plan Apochromat 100x 1.3NA oil-immersion lens.

Image analysis was done in FIJI/ImageJ2 ^{60,61} and Python 3. Cell segmentation was conducted using custom Python scripts making use of the Unet segmentation architecture ⁶² for deep learning and implemented with Pytorch ⁶³.

Mean fluorescence intensity plots were generated by segmenting the cells using the chlorophyll autofluorescence channel, rotating the cells such that the medial axis was horizontal, rescaling the dimensions to 500 x 200 pixels to ensure consistent boundaries, and finally averaging of the RbcS-mNG pixel intensity from each cell in the collection of images from its respective induction condition and timepoint. Foci locations were determined with a peak-finding algorithm using the Python package Photutils.⁶⁴ To calculate the amount of RbcS-mNG in the cytosol, the fluorescence signal from foci was removed using a local adaptive threshold to mask the foci (see examples in Figures S12, S13). Cell size was accounted for by dividing the cumulative pixel intensity from each cell by the number of pixels.

Immunofluorescence

For FtsZ localization, cells were first fixed in 2% glutaraldehyde + 2% paraformaldehyde (Electron Microscopy Sciences) in phosphate buffer, pH 7.4 for 15 mins at room temperature. After washing three times in phosphate buffered saline (PBS) supplemented with 0.01% Tween-20, samples were treated with 0.05% Triton X-100 in PBS for 15 min, washed twice, and permeabilized for 30 min at 37°C with 0.2 mg ml⁻¹ lysozyme dissolved in Tris-HCl, pH 7.5, 10 mM EDTA, and washed twice. After blocking with 5% bovine serum albumin in PBS (blocking buffer) for 1 hour, cells were labelled overnight at 4°C with anti-Anabaena FtsZ antibodies (Agrisera, AS07 217) diluted 1:250 in blocking buffer. Cells were then washed three times with blocking buffer, followed by secondary staining for 1 hour at room temperature with goat anti-rabbit IgG DyLight 488 (Thermo-Fisher Scientific, 35552) diluted 1:1000 in blocking buffer.

Immunoblotting

Cells were pelleted by centrifugation at 3,700 × g, 4°C for 15 minutes, the supernatant was discarded, and pellets were stored at -80°C until needed. Cell pellets were resuspended in precooled 50 mM Tris pH 7.4, 1 mM EDTA, 10 mM dithiothreitol (DTT), 0.1% Triton X-100, and Halt protease and phosphatase inhibitor cocktail (ThermoFisher). Cell lysis was performed with sonication at 4°C for 20 cycles of 30 s on/ 10 s off at 45% amplitude and cell debris was removed via centrifugation for 10 minutes at 13,000 × g, 4°C. Samples were denatured in Laemmli loading buffer by incubation at 95°C for 10 mins. The samples were then subjected to electrophoresis at 30 mA in Any kD™ Mini-PROTEAN® TGX™precast protein gels (Bio-Rad). Protein transfer was conducted using the

Trans-Blot Turbo Transfer System (Bio-Rad) onto a polyvinylidene difluoride (PVDF) membrane with Towbin Buffer for transferring (25 mM Tris, 192 mM glycine, 20% (v/v) methanol, 0.1% SDS). The membrane was blocked for 1 hour at room temperature with 5% Blotto in TBS-T (19 mM TRIS, 137 mM NaCl, 2.7 mM KCl, 0.2% Tween 20). For RbcS detection, a rabbit α-CbbS primary antibody (PHY5240A, PhytoAB) was incubated overnight at 4°C in blocking buffer at a 1:1000 dilution. The blot was then washed quickly 3x in TBS-T, followed by two 15-minute washes at room temperature. The secondary antibody, goat α-rabbit IgG + HRP (G21234, Invitrogen), was added and incubated at a dilution of 1:20,000 for 1 hour at room temperature before washing. For FLAG-*mf-lon* detection, a mouse α-FLAG (DYKDDDDK) primary antibody (1:1000 dilution: LT0420, Lifetein) and secondary antibody, chicken α-mouse IgG + HRP (1:5000 dilution: SA1-72021, ThermoFisher Scientific) were substituted and blots were processed as above. Enhanced chemiluminescent substrate was used for imaging (SuperSignal TM West Femto, ThermoFisher Scientific).

Photosynthetic parameters

Measurement of photosynthetic parameters was performed on a custom-built fluorimeter with a Z Color Line light emitting diode (LED, Luxeon) pulsed measuring beam (emission peak at 590 nm)⁶⁵. The sample was illuminated with actinic light using three different intensities: 100, 275 and 500 μ mol photons m⁻² s⁻¹ of photosynthetic photon flux density (460 nm peak emission). Chlorophyll fluorescence was filtered with a long-pass RG-695 nm filter in front of the detector. The relative yields of chlorophyll fluorescence were measured under steady-state illumination (F_s), during ~1.5 s saturating pulses of actinic light (F'_m) and after exposure to ~2 s of far-red illumination to obtain minimal fluorescence (F'₀). From these fluorescence yields, the quantum yield of Photosystem II (PSII, Φ _{II}) and the coefficient of photochemical quenching (q_P) were calculated ^{66,67}:

$$\phi_{II} = \frac{F_m' - F_s}{F_m'}$$

$$q_P = \frac{F_m' - F_s}{F_m' - F_o'}$$

Flow cytometry

All flow cytometry measurements were performed on exponential cultures (*i.e.*, cells backdiluted daily as described above and between 0.3 and 1.5 OD₇₅₀). Live-cell measurements directly utilized cell suspensions diluted 1:1000 in BG-11, while time course experiments utilized cells frozen at -80°C in BG-11 containing 3.5 mM dimethyl sulfoxide. Samples were measured on an LSRII Flow Cytometer (BD Biosciences) using the FITC-A/PerCP-Cy5 channels for mNeonGreen and chlorophyll *a* autofluorescence, respectively. Samples were thresholded using the PerCP-Cy5 channel to remove debris and noise, and >100,000 cells were measured per sample type. Data was analyzed in Python with the Cytoflow package (https://bpteague.github.io/cytoflow/).

Proteomics

Cell cultures (100 mL) were grown in 250 mL baffled flasks (Corning) and *mf-lon* expression was induced with 1 mM theophylline. At 2 or 4 hours after induction, samples were pelleted by centrifugation at 3,700 × g, 4°C, resuspended in Tris buffer (50 mM Tris-HCL, 10 mM CaCl₂, 0.1% Triton X-100, pH 7.6) with Halt protease and phosphatase inhibitor cocktail (ThermoFisher) and lysed with a French press. After centrifugation of the crude lysate (17,000 × g, 4°C), proteins were then precipitated using acetone (-20°C, overnight) before proteolytic digestion, Tandem Mass Tag labelling, and LC/MS/MS analysis. 2-hour, and 4-hour samples induced with 1 mM theophylline were compared against uninduced controls in Scaffold (Proteome Software, Portland, OR USA) using a Kruskal-Wallis Test (p < 0.05) with a Benjamani-Hochberg stepdown (p < 0.00187, **Supplemental Table 1**). Gene ontology associations were generated with ClueGO⁶⁸, a Cytoscape plugin⁵². See Supplemental Methods for additional details.

Statistical analysis and experimental replicates

Unless noted otherwise, error bars indicate standard deviation. Geometric mean and standard deviation are reported for flow cytometry data. Three independent biological replicates were conducted for each experiment, unless otherwise noted. P-values were calculated from independent student's t-tests, unless described differently.

DATA AVAILABILITY

All data generated in this study are available in the main text and supplementary figures. Raw datasets that support the findings of this study are available from the corresponding author upon request. Flow cytometry data are deposited in FlowRepository: FR-FCM-Z3CM, FR-FCM-Z3D8. Proteomics data are deposited in ProteomeXchange with identifier PXD023591. Plasmid maps are available at https://github.com/ddcyanolab/orthogonal-degron-system.

SUPPORTING INFORMATION

The Supporting Information contains 13 supplementary figures, 1 table, and expanded description of the methodology of proteomics analysis. Additionally, an excel spreadsheet detailing proteomics data output from Scaffold is contained. Figure S1: Flow cytometry of *mf-lon* induction, Figure S2: Western blot showing *mf-lon* accumulation, Figure S3: mNG-PDT downregulation timecourse, Figure S4: Site-directed mutagenesis of the PDT, Figure S5: Effect of theophylline on growth rate, Figure S6: Cartoon of expected phenotypes, Figure S7: Alternative FtsZ mutant hyperelongation, Figure S8: Control of cell elongation with truncated PDT, Figure S9: Genetic constructs for carboxysome manipulation, Figure S10: CcmL downregulation, Figure S11: Redistribution of carboxysome spacing after CcmO downregulation, Figure S12: Representative cell segmentations, Figure S13: Cytosolic RbcS depletion after CcmO downregulation, Table S1: Gene ontology enrichment analysis of *mf-lon* off-target proteins, Methods S1: Proteomics extended methods.

ACKNOWLEDGEMENT

We thank Dr. Maria Santos-Merino for assistance with cyanobacterial transformations, photosynthetic parameter measurement, and helpful discussions. We thank Drs. Jincheng Huang, Eric Young, Joshua MacCready, and Amit Singh, and Lisa Yun for helpful discussions. We thank Dr. Doug Whitten for proteomics sample processing and guidance with the respective data analysis.

FUNDING

This work was funded primarily by National Science Foundation Grant #1517241 (to K.W.O. and D.C.D), with supplementary funding from Department of Energy Grant #DE-FG02-91ER20021 (to D.C.D) at the MSU DOE-PRL. Additional support for the research was provided by NSF Award # 1845463 (to D.C.D).

CONFLICT OF INTEREST

The authors declare no conflict of interest.

TABLES AND FIGURES

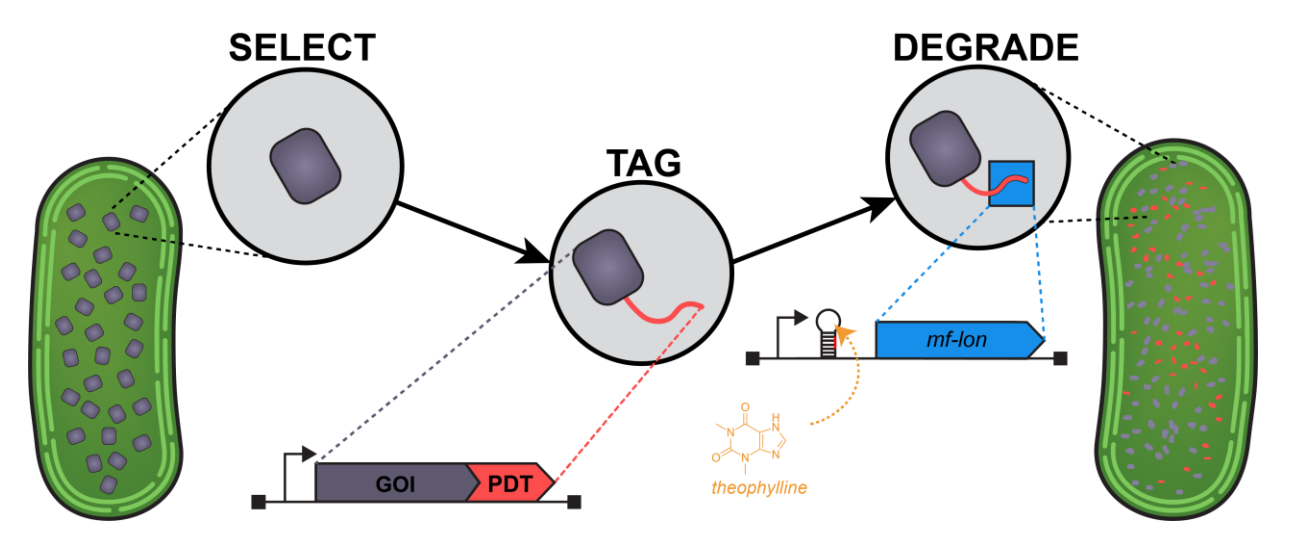


Figure 1: Overview diagram of the tunable degradation system from *M. florum*. The coding sequence for a gene of interest (GOI) is appended with a 84 bp (26 AA) protein degradation tag (PDT). Upon induction of *mf-lon* protease with theophylline, the PDT is recognized by *mf-lon* and the protein is degraded.

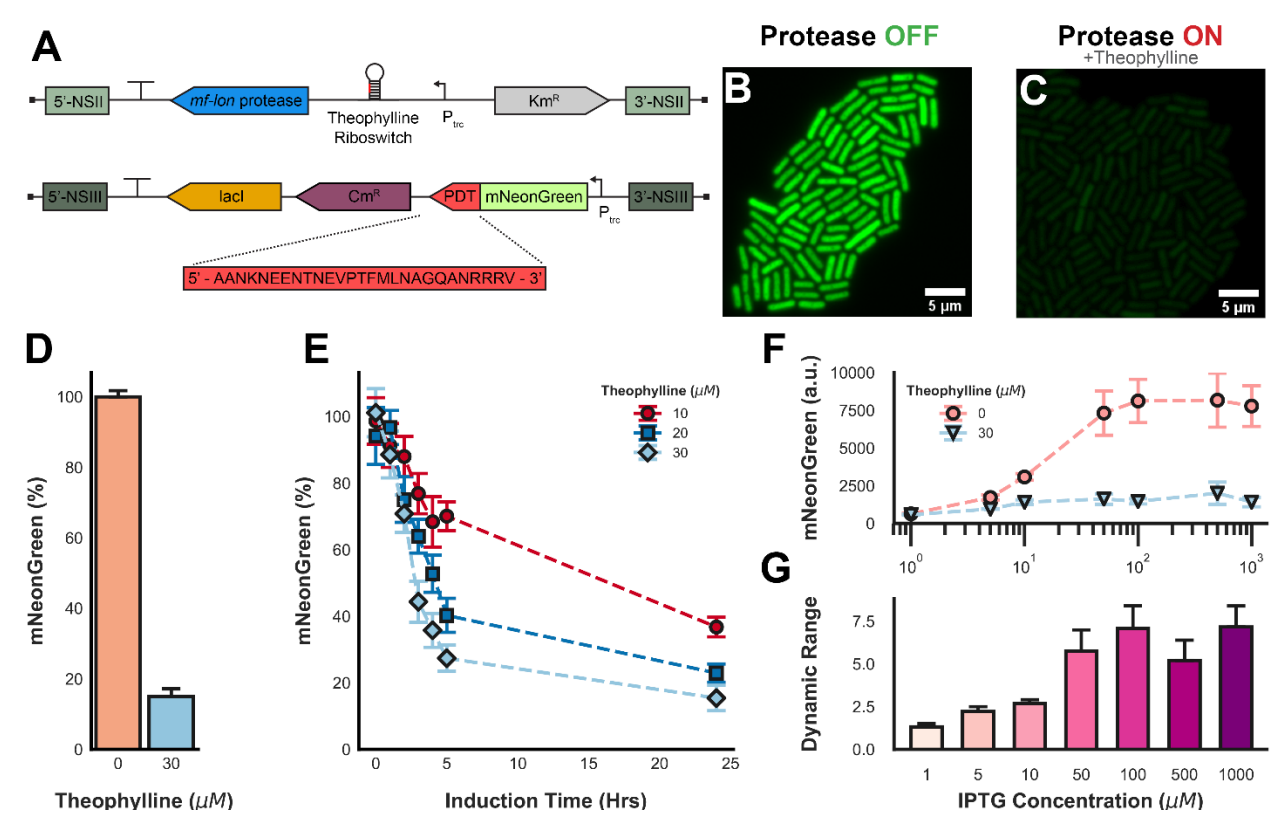
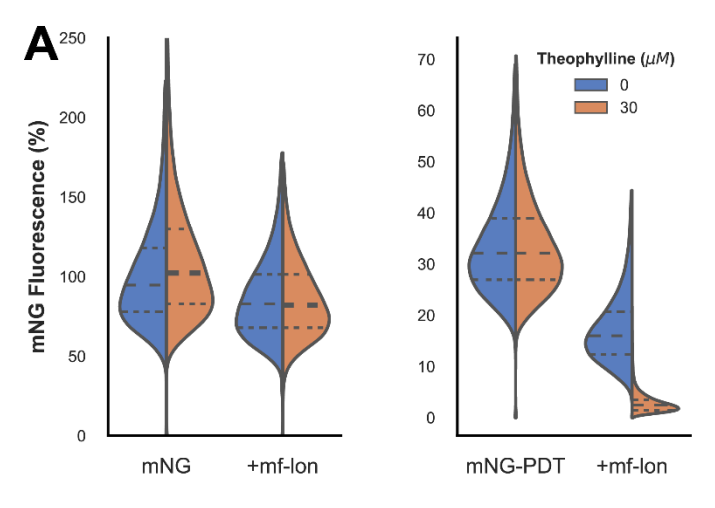
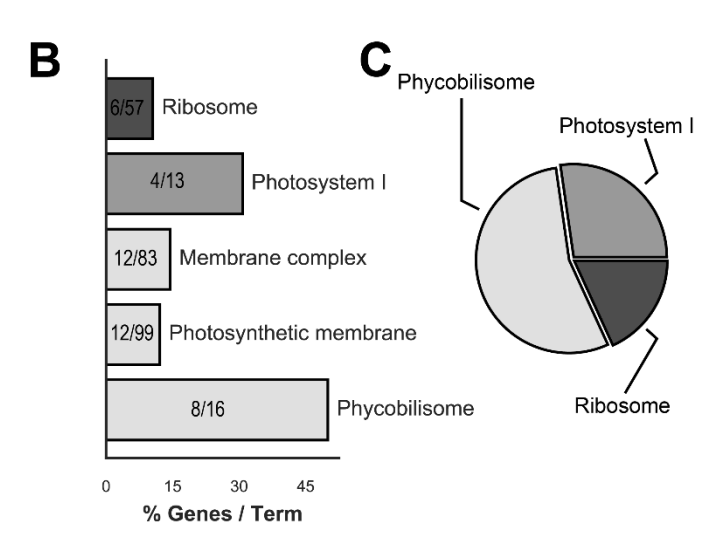


Figure 2: Characterization of *mf-lon* using a reporter. A) Genetic constructs used to express the fluorescent reporter protein, mNeonGreen (mNG), and lon protease (*mf-lon*). B) mNG fluorescence is diminished after IPTG induction of *mf-lon*. C) PDT-tagged mNG is degraded after expression of *mf-lon* (30 µM theophylline). D) Flow cytometry data shows a 7-fold difference in normalized mNG fluorescence (*mf-lon* OFF:ON). E) Near complete protein degradation within hours of *mf-lon* induction. F) mNG reporter level does not affect the extent of degradation by *mf-lon*. G) The dynamic range in mNG between *mf-lon* OFF/ON scales with mNG level, but plateaus under high (> 100 µM IPTG) induction. Panels C/D/F/G are 24 hours post induction. Data in panels D-G were collected via flow cytometry. Strain: mNG-PDT/*mf-lon* (DD309).





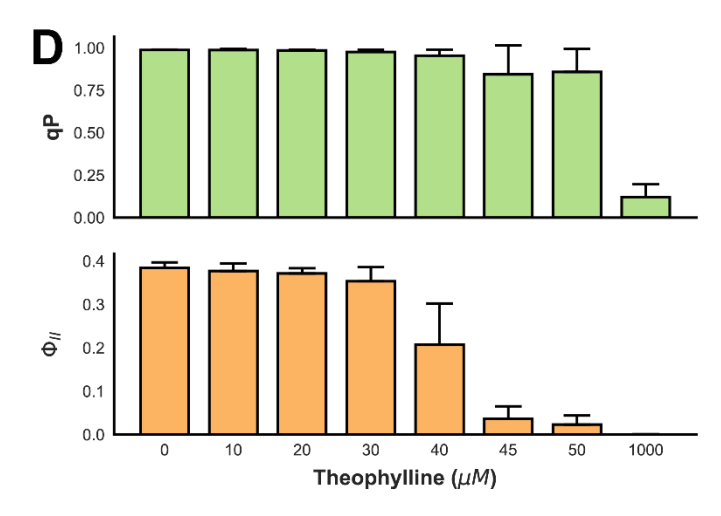


Figure 3: Off-target effects of mf-lon in S. elongatus. A) PDT is recognized by native proteases in S. elongatus. Fluorescence intensities of different reporter constructs as indicated were normalized against the mean fluorescence intensity from the uninduced mNG reporter (0 mM theophylline). B) Proteins related to photosynthesis are nonspecifically degraded by mf-lon. The number of genes identified as significantly downregulated by 1 mM theophylline induction of mf-lon and total genes associated with each Gene Ontology (GO) term are shown in each bar. C) The majority of these proteins are associated with the phycobilisomes. Phycobilisome-related genes include the GO terms membrane complex, photosynthetic membrane, and phycobilisome, and both B/C are color coded to reflect these categories. D) The appropriate level of *mf-lon* induction to minimize off-target effects was optimized based on sensitive photosynthetic parameters including \$\phi II (quantum efficiency of photosystem II) and qP (estimate of photosystem II "openness"). B/C) Cultures were treated with 1 mM theophylline for 2-4 hours to induce mf-lon expression prior to proteomics analysis. A/D) Cultures were induced with the indicated [theophylline] for 24 hours before analysis. Strains: A) mNG (DD306), mNG/mf-lon (DD308), mNG-PDT (DD307), mNG-PDT/mf-lon (DD309), B-D)mf-Ion (DD206).

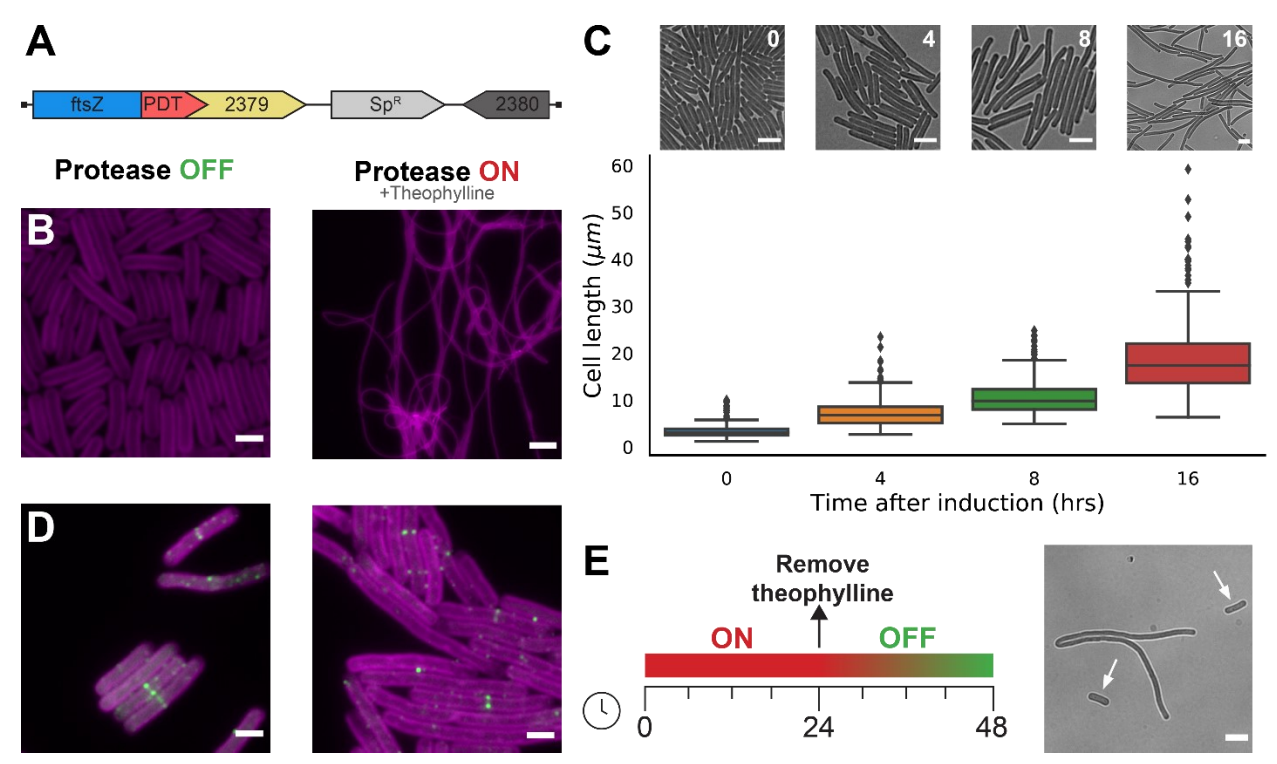


Figure 4: Targeted degradation of native FtsZ leads to rapid cell division arrest and onset of cell elongation. A) Cartoon schematic of genetic construct used for native knock-in of the PDT on the C-terminus of FtsZ. A 2 bp overlap between the stop and start codons of ftsZ and Synpcc7942_2379, respectively, was maintained with the PDT stop codon, as indicated in the diagram. B) Cells elongate after induction (30 μM theophylline) of *mf-lon* for 24 hours (chlorophyll autofluorescence, magenta). C) Cell elongation can be observed within hours of *mf-lon* induction. D) FtsZ immunofluorescence (green) shows diminished levels of FtsZ and Z-ring assemblies after *mf-lon* induction. E) Cell division returns within 24 hours of theophylline removal. Arrows indicate newly budded cells with WT length. Scale bars are: B) 2 (left) and 15 μm (right), C) 5 μm, D) 2 μm, and E) 5 μm. Strain: FtsZ-PDT*/ *mf-lon* (DD347).

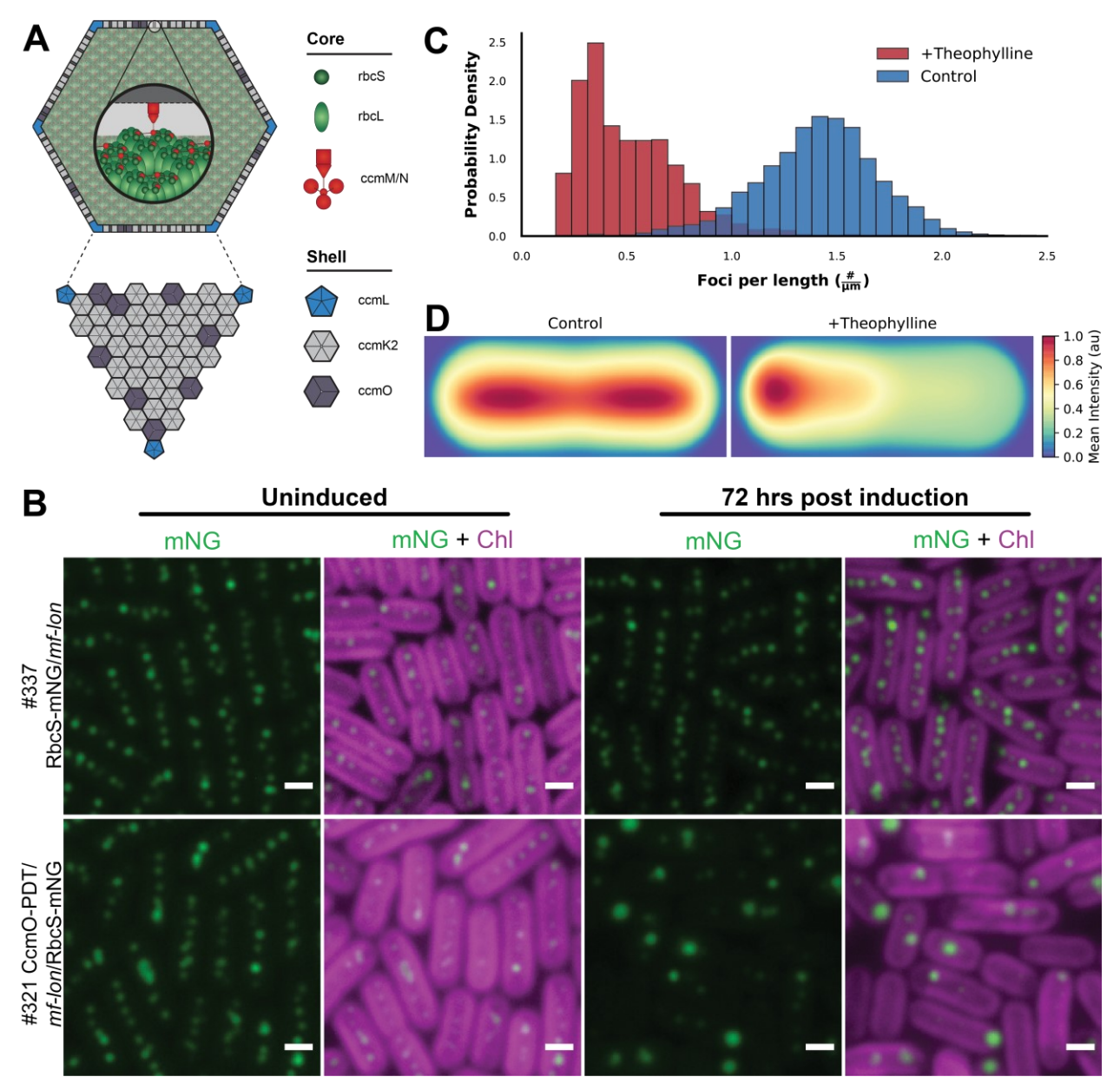


Figure 5: Targeting the carboxysome. A) Diagram of selected internal and shell proteins associated with the carboxysome. B) Fluorescence microscopy of *S. elongatus* cells with either *mf-lon* protease and RbcS-mNG reporter (top row) or natively degron tagged CcmO in addition to the previous two transformations (bottom row). Rubisco reporter (mNG, shown in green) and overlay (mNG + chlorophyll autofluorescence (Chl), shown in magenta). C) Histogram of the number of foci (fluorescent puncta representing carboxysomes) per unit cell length of control (no *mf-lon* induction) vs 30 μM theophylline *mf-lon* induction after 72 hours. D) Mean fluorescence intensity mapped to a representative cell. C/D) n = 6,838 (control, DD321 without induction), n = 2,637 (+theophylline, DD321). Strains: RbcS-mNG/mf-lon (DD337), CcmO-PDT/mf-lon/RbcS-mNG (DD321). Scale bars are 1 μm. B-D) Either 0 μM (Uninduced/Control) or 30 μM (+theophylline) theophylline was used for the induction conditions shown.

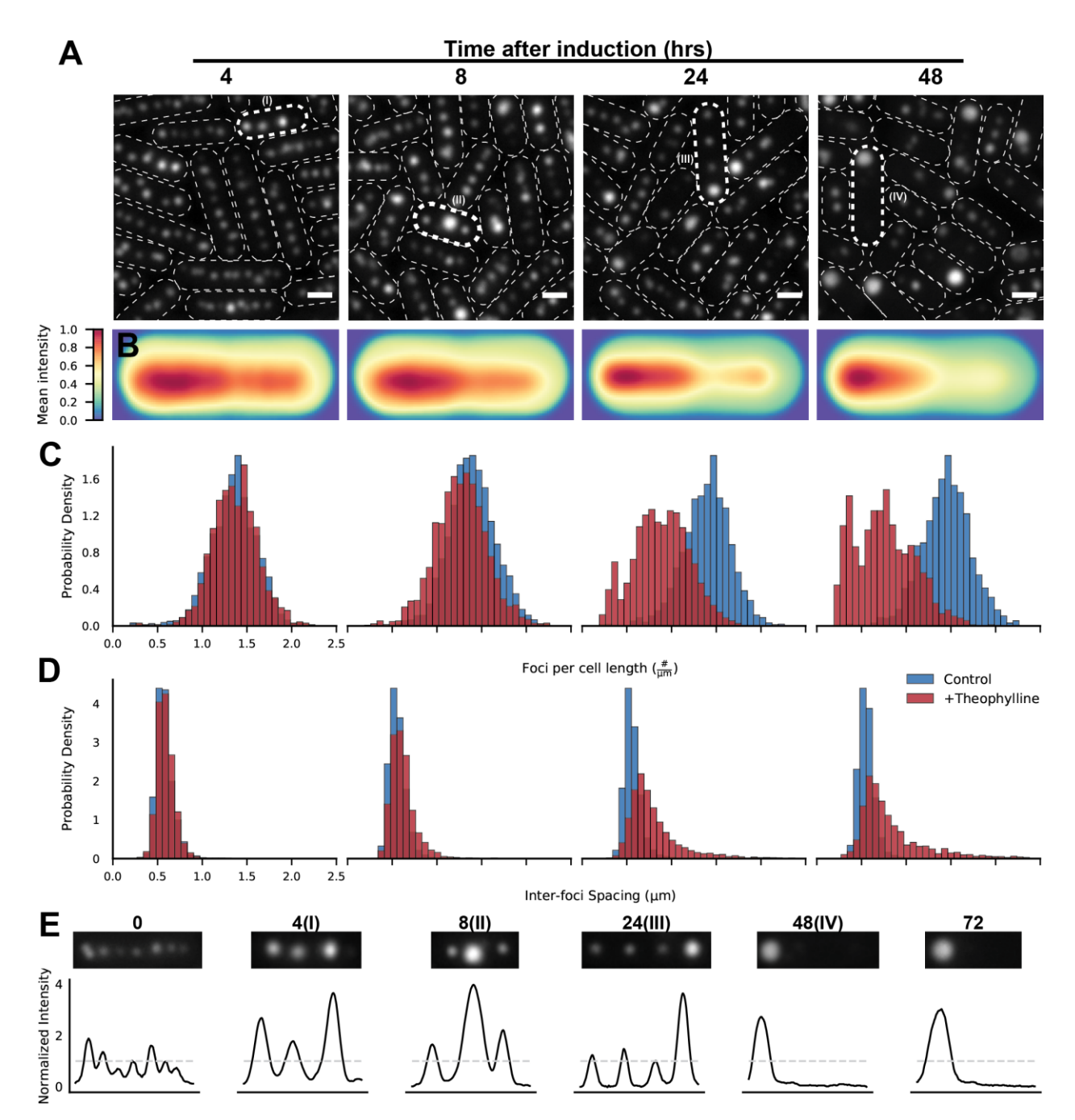


Figure 6: Carboxysome reorganization after *mf-lon* induction. A) Foci aggregation takes place within 24 hours, with phenotype penetrance increasing until 72 hours. B) Mean fluorescence intensity mapped to a representative cell shows the gradual polar aggregation. C) Foci per unit cell length confirms the decrease in foci over time with *mf-lon* induction. D) Inter-foci spacing is disrupted after *mf-lon* induction. E) Carboxysomes reorganize within 72 hours following *mf-lon* induction and Rubisco aggregates into a singular polar body. Line profiles through representative cells show the fluorescence intensity peaks (foci) normalized to average peak intensity in uninduced control samples. Dashed grey line indicates a value of 1. Subpanel titles indicate the hours post induction (hpi). Cells taken from image fields in panel A are

indicated with Roman numerals in parenthesis following the hpi. A/E) Scale bars are 1 um. B/C/D) n > 3,800. Strain: CcmO-PDT/mf-lon/RbcS-mNG (DD321). Except where denoted "Control", samples were induced with 30 μ M theophylline.

Table 1: List of plasmids used in this study

Number	Name	Description ^{a,b}	Reference ^c
3	pAM2314	Neutral site 1 shuttle vector; Sp ^r	104
112	pHN1_lacUV5	Neutral site 3 shuttle vector; Cm ^r ; P _{trc}	52
511	pEYN12	pBluescript II KS(+) with NSII flanking	81
		regions;P _{trc} ::riboswitch-E*:: <i>luc</i> +; Km ^r ; (Amp ^r)	
673	pEYN12-mflon	pEYN12 with lon protease from Mesoplasma florum;	This work
		Km ^r ; (Amp ^r)	
680	pFtsZ-PDT Native FtsZ C-terminal fusion with PDT; Sp ^r		This work
685	pAM2314-RbcS-	pAM2314 with P _{rbcs} ::rbcS fused to mNeonGreen; Cm ^r	81
	mNG		
847	pHN1_lacUV5-mNG	pHN1_lacUV5-mNG pHN1_lacUV5 with mNeonGreen; Cm ^r	
848	pHN1_lacUV5-mNG-	pHN1_lacUV5 with mNeonGreen and C-terminally	This work
	PDT	fused PDT; Cm ^r	
849	pCcmO-StrepII-PDT Native CcmO fusion with a StrepII tag and PDT; Spr		This work
850	pHN1_lacUV5-mNG-	pHN1_lacUV5-mNG-PDT with A1D PDT mutation; Cm ^r	This work
	PDT(A1D)		
851	pHN1_lacUV5-mNG-	pHN1_lacUV5-mNG-PDT with A2D PDT mutation; Cm ^r	This work
	PDT(A2D)		
852	pHN1_lacUV5-mNG-	pHN1_lacUV5-mNG-PDT with N3D PDT mutation; Cm ^r	This work
	PDT(N3D)		
853	pHN1_lacUV5-mNG-	pHN1_lacUV5-mNG-PDT with K4D PDT mutation; Cm ^r	This work
	PDT(K4D)		
854	pHN1_lacUV5-mNG-	pHN1_lacUV5-mNG-PDT with random mutations at the	This work
	PDT(RRRV24-	PDT C-terminus RRRV24-27NNNN; Cm ^r	
	27NNNN)		
967	pCcmL-PDT	pCcmL-PDT Native CcmL C-terminal fusion with PDT; Sp ^r	
970	pFtsZ-PDT(del1-13)	Native FtsZ C-terminal fusion with truncated PDT, first	This work
		13 residues deleted; Sp ^r	
1008	FLAG-mf-lon	N-terminal FLAG fusion to mf-lon protease); Km ^r ;	This work
		(Amp ^r)	
			1

^aCm^r, chloramphenicol resistance; Km^r, kanamycin resistance; Sp^r, spectinomycin resistance; Amp^r, ampicillin resistance

^bNSI, neutral site 1; NSII, neutral site 2; NSIII, neutral site 3.

°PCC, Pasteur Culture Collection.

Table 2: List of strains used in this study

Strain	Strain	Genotype ^{a,b}	Plasmids
Name	Number		Used
wt		Wild type strain Synechococcus elongatus PCC 7942	
mf-lon	DD206	Mf-lon protease	673
mNG	DD306	mNeonGreen reporter	847
mNG-	DD307	mNeonGreen reporter with C-terminal PDT fusion	848
PDT			
mNG/ mf-	DD308	mNeonGreen reporter with mf-lon protease	847,673
lon			
mNG-	DD309	mNeonGreen reporter with C-terminal PDT fusion with mf-lon	848,673
PDT/ mf-		protease	
lon			
FtsZ-	DD312	Native FtsZ-PDT with mf-lon protease	680,673
PDT/ mf-			
lon			
CcmO-	DD313	Native CcmO-PDT with mf-lon protease	673,849
PDT/mf-			
lon			
CcmO-	DD314	Native CcmO with C-terminal PDT fusion	849
PDT			
mNG-	DD315	mNeonGreen reporter with C-terminal fusion of modified PDT	850
PDT(A1D		(A1D)	
)			
mNG-	DD316	mNeonGreen reporter with C-terminal fusion of modified PDT	851
PDT(A2D		(A2D)	
)			
mNG-	DD317	mNeonGreen reporter with C-terminal fusion of modified PDT	852
PDT(N3D		(N3D)	
)			

mNG-	DD318	mNeonGreen reporter with C-terminal fusion of modified PDT	853
PDT(K4D		(K4D)	
)			
mNG-	DD319	mNeonGreen reporter with C-terminal fusion of modified PDT	673,851
PDT(A2D		(A2D) with mf-lon protease	
)/mf-lon			
mNG-	DD320	mNeonGreen reporter with C-terminal fusion of modified PDT	673,852
PDT(N3D		(N3D) with mf-lon protease	
)/mf-lon			
CcmO-	DD321	Native CcmO-PDT with mf-lon protease and RbcS	673,685,8
PDT/mf-		mNeonGreen fusion carboxysome reporter	49
lon/RbcS-			
mNG			
mNG-	DD322	mNeonGreen reporter with C-terminal fusion of modified PDT	673,850
PDT(A1D		(A1D) with mf-lon protease	
)/mf-lon			
mNG-	DD324	mNeonGreen reporter with C-terminal fusion of modified PDT	673,853
PDT(K4D		(K4D) with mf-lon protease	
)/mf-lon			
RbcS-	DD337	RbcS mNeonGreen fusion carboxysome reporter with mf-lon	673,685
mNG/mf-		protease	
lon			
FtsZ-PDT	DD346	Native FtsZ-PDT	680
FtsZ-	DD347	Native FtsZ with truncated C-terminal PDT fusion (PDT*) and	673,970
PDT*/ mf-		mf-lon protease	
lon			
CcmL-	DD348	Native CcmL-PDT with mf-lon protease and RbcS	685, 967,
PDT/mf-		mNeonGreen fusion carboxysome reporter	673
lon/RbcS-			
mNG			
FLAG-mf-	DD352	N-terminal FLAG3x fusion to mf-lon protease	1008
lon			

REFERENCES

- (1) Casella, S.; Huang, F.; Mason, D.; Zhao, G. Y.; Johnson, G. N.; Mullineaux, C. W.; Liu, L. N. Dissecting the Native Architecture and Dynamics of Cyanobacterial Photosynthetic Machinery. *Molecular Plant* 2017, *10* (11), 1434–1448. https://doi.org/10.1016/j.molp.2017.09.019.
- (2) Fraser, J. M.; Tulk, S. E.; Jeans, J. A.; Campbell, D. A.; Bibby, T. S.; Cockshutt, A. M. Photophysiological and Photosynthetic Complex Changes during Iron Starvation in Synechocystis Sp. PCC 6803 and Synechococcus Elongatus PCC 7942. *PLoS ONE* 2013, 8 (3). https://doi.org/10.1371/journal.pone.0059861.
- (3) Salem, K.; van Waasbergen, L. G. Photosynthetic Electron Transport Controls Expression of the High Light Inducible Gene in the Cyanobacterium Synechococcus Elongatus Strain PCC 7942. *Plant and Cell Physiology* **2004**, *45* (5), 651–658. https://doi.org/10.1093/pcp/pch072.
- (4) Shaku, K.; Shimakawa, G.; Hashiguchi, M.; Miyake, C. Reduction-Induced Suppression of Electron Flow (RISE) in the Photosynthetic Electron Transport System of Synechococcus Elongatus PCC 7942. *Plant and Cell Physiology* 2016, 57 (7), 1443–1453. https://doi.org/10.1093/pcp/pcv198.
- (5) Taton, A.; Erikson, C.; Yang, Y.; Rubin, B. E.; Rifkin, S. A.; Golden, J. W.; Golden, S. S. The Circadian Clock and Darkness Control Natural Competence in Cyanobacteria. *Nature communications* 2020, *11* (1), 1688. https://doi.org/10.1038/s41467-020-15384-9.
- (6) van Waasbergen, L. G.; Dolganov, N.; Grossman, A. R. NblS, a Gene Involved in Controlling Photosynthesis-Related Gene Expression during High Light and Nutrient Stress in Synechococcus Elongatus Pcc 7942. *Journal of Bacteriology* 2002, 184 (9), 2481–2490. https://doi.org/10.1128/JB.184.9.2481-2490.2002.
- (7) Cohen, S. E.; McKnight, B. M.; Golden, S. S. Roles for ClpXP in Regulating the Circadian Clock in Synechococcus Elongatus. *Proceedings of the National Academy of Sciences* 2018, 115 (33), E7805–E7813. https://doi.org/10.1073/pnas.1800828115.
- (8) Ditty, J. L.; Canales, S. R.; Anderson, B. E.; Williams, S. B.; Golden, S. S. Stability of the Synechococcus Elongatus PCC 7942 Circadian Clock under Directed Anti-Phase Expression of the Kai Genes. *Microbiology* 2005, 151 (8), 2605–2613. https://doi.org/10.1099/mic.0.28030-0.
- (9) Wishiwaki, T.; Satomi, Y.; Nakajima, M.; Lee, C.; Kiyohara, R.; Kageyama, H.; Kitayama, Y.; Temamoto, M.; Yamaguchi, A.; Hijikata, A.; Go, M.; Iwasaki, H.; Takao, T.; Kondo, T. Role of KaiC Phosphorylation in the Circadian Clock System of Synechococcus Elongatus PCC 7942. Proceedings of the National Academy of Sciences of the United States of America 2004, 101 (38), 13927–13932. https://doi.org/10.1073/pnas.0403906101.

- (10) Cameron, J. C.; Wilson, S. C.; Bernstein, S. L.; Kerfeld, C. A. Biogenesis of a Bacterial Organelle: The Carboxysome Assembly Pathway. *Cell* 2013, 155 (5), 1131–1140. https://doi.org/10.1016/j.cell.2013.10.044.
- (11) Chen, A. H.; Robinson-Mosher, A.; Savage, D. F.; Silver, P. A.; Polka, J. K. The Bacterial Carbon-Fixing Organelle Is Formed by Shell Envelopment of Preassembled Cargo. *PLoS ONE* 2013, 8 (9), 1–13. https://doi.org/10.1371/journal.pone.0076127.
- (12) Huang, F.; Vasieva, O.; Sun, Y.; Faulkner, M.; Dykes, G. F.; Zhao, Z.; Liu, L. N. Roles of RBcX in Carboxysome Biosynthesis in the Cyanobacterium Synechococcus Elongatus PCC7942. Plant Physiology 2019, 179 (1), 184–194. https://doi.org/10.1104/pp.18.01217.
- (13) Orus, M. I.; Rodriguez, M. L.; Martinez, F.; Marco, E. Biogenesis and Ultrastructure of Carboxysomes from Wild Type and Mutants of Synechococcus Sp. Strain PCC 7942. *Plant physiology* 1995, 107 (4), 1159–1166. https://doi.org/107/4/1159 [pii].
- (14) Sun, Y. Investigating the Functional and Structural Modulation of Carboxysomes in Synechococcus Elongatus PCC7942. 2018, No. September.
- (15) Abramson, B. W.; Lensmire, J.; Lin, Y. T.; Jennings, E.; Ducat, D. C. Redirecting Carbon to Bioproduction via a Growth Arrest Switch in a Sucrose-Secreting Cyanobacterium. *Algal Research* 2018, 33 (January), 248–255. https://doi.org/10.1016/j.algal.2018.05.013.
- (16) Chwa, J. W.; Kim, W. J.; Sim, S. J.; Um, Y.; Woo, H. M. Engineering of a Modular and Synthetic Phosphoketolase Pathway for Photosynthetic Production of Acetone from CO2 in Synechococcus Elongatus PCC 7942 under Light and Aerobic Condition. *Plant Biotechnology Journal* 2016, 14 (8), 1768–1776. https://doi.org/10.1111/pbi.12536.
- (17) Hirokawa, Y.; Dempo, Y.; Fukusaki, E.; Hanai, T. Metabolic Engineering for Isopropanol Production by an Engineered Cyanobacterium, Synechococcus Elongatus PCC 7942, under Photosynthetic Conditions. *Journal of Bioscience and Bioengineering* 2017, 123 (1), 39–45. https://doi.org/10.1016/j.jbiosc.2016.07.005.
- (18) Li, X.; Shen, C. R.; Liao, J. C. Isobutanol Production as an Alternative Metabolic Sink to Rescue the Growth Deficiency of the Glycogen Mutant of Synechococcus Elongatus PCC 7942. *Photosynthesis Research* 2014, 120 (3), 301–310. https://doi.org/10.1007/s11120-014-9987-6.
- (19) Weiss, T. L.; Young, E. J.; Ducat, D. C. A Synthetic, Light-Driven Consortium of Cyanobacteria and Heterotrophic Bacteria Enables Stable Polyhydroxybutyrate Production. *Metabolic Engineering* 2017, 44 (September), 236–245. https://doi.org/10.1016/j.ymben.2017.10.009.
- (20) Rubin, B. E.; Wetmore, K. M.; Price, M. N.; Diamond, S.; Shultzaberger, R. K.; Lowe, L. C.; Curtin, G.; Arkin, A. P.; Deutschbauer, A.; Golden, S. S. The Essential Gene Set of a Photosynthetic Organism. *Proceedings of the National Academy of Sciences* 2015, 112 (48), E6634–E6643. https://doi.org/10.1073/pnas.1519220112.

- (21) Sun, T.; Li, S.; Song, X.; Diao, J.; Chen, L.; Zhang, W. Toolboxes for Cyanobacteria: Recent Advances and Future Direction. *Biotechnology Advances* **2018**, *36* (4), 1293–1307. https://doi.org/10.1016/j.biotechadv.2018.04.007.
- (22) Teng, X.; Dayhoff-Brannigan, M.; Cheng, W. C.; Gilbert, C. E.; Sing, C. N.; Diny, N. L.; Wheelan, S. J.; Dunham, M. J.; Boeke, J. D.; Pineda, F. J.; Hardwick, J. M. Genome-Wide Consequences of Deleting Any Single Gene. *Molecular Cell* **2013**, *52* (4), 485–494. https://doi.org/10.1016/j.molcel.2013.09.026.
- (23) Reznikoff, W. S. Transposon Tn5. Annual Review of Genetics. 2008, pp 269–286. https://doi.org/10.1146/annurev.genet.42.110807.091656.
- (24) Barquist, L.; Boinett, C. J.; Cain, A. K. Approaches to Querying Bacterial Genomes with Transposon-Insertion Sequencing. RNA Biology. Taylor and Francis Inc. 2013, pp 1161– 1169. https://doi.org/10.4161/rna.24765.
- (25) Hayes, F. Transposon-Based Strategies for Microbial Functional Genomics and Proteomics. Annual Review of Genetics. 2003, pp 3–29. https://doi.org/10.1146/annurev.genet.37.110801.142807.
- (26) Gordon, G. C.; Korosh, T. C.; Cameron, J. C.; Markley, A. L.; Begemann, M. B.; Pfleger, B. F. CRISPR Interference as a Titratable, Trans-Acting Regulatory Tool for Metabolic Engineering in the Cyanobacterium Synechococcus Sp. Strain PCC 7002. *Metabolic Engineering* 2016, 38, 170–179. https://doi.org/10.1016/j.ymben.2016.07.007.
- (27) Huang, C. H.; Shen, C. R.; Li, H.; Sung, L. Y.; Wu, M. Y.; Hu, Y. C. CRISPR Interference (CRISPRi) for Gene Regulation and Succinate Production in Cyanobacterium S. Elongatus PCC 7942. *Microbial Cell Factories* 2016, 15 (1), 1–11. https://doi.org/10.1186/s12934-016-0595-3.
- Yao, L.; Cengic, I.; Anfelt, J.; Hudson, E. P. Multiple Gene Repression in Cyanobacteria Using CRISPRi. ACS Synthetic Biology 2016, 5 (3), 207–212. https://doi.org/10.1021/acssynbio.5b00264.
- (29) Zheng, Y.; Su, T.; Qi, Q. Microbial CRISPRi and CRISPRa Systems for Metabolic Engineering. Biotechnology and Bioprocess Engineering. Korean Society for Biotechnology and Bioengineering August 1, 2019, pp 579–591. https://doi.org/10.1007/s12257-019-0107-5.
- (30) Copeland, M. F.; Politz, M. C.; Johnson, C. B.; Markley, A. L.; Pfleger, B. F. A Transcription Activator-like Effector (TALE) Induction System Mediated by Proteolysis. *Nature Chemical Biology* **2016**, *12* (4), 254–260. https://doi.org/10.1038/nchembio.2021.
- (31) Farrell, C. M.; Grossman, A. D.; Sauer, R. T. Cytoplasmic Degradation of SsrA-Tagged Proteins. *Molecular Microbiology* **2005**, *57* (6), 1750–1761. https://doi.org/10.1111/j.1365-2958.2005.04798.x.

- (32) Gottesman, S.; Roche, E.; Zhou, Y. N.; Sauer, R. T. The ClpXP and ClpAP Proteases Degrade Proteins with Carboxy-Terminal Peptide Tails Added by the SsrA-Tagging System. *Genes and Development* 1998, 12 (9), 1338–1347. https://doi.org/10.1101/gad.12.9.1338.
- (33) Janssen, B. D.; Hayes, C. S. The TmRNA Ribosome-Rescue System. Advances in Protein Chemistry and Structural Biology. 1st ed. Elsevier Inc. 2012, pp 151–191. https://doi.org/10.1016/B978-0-12-386497-0.00005-0.
- (34) Landry, B. P.; Stöckel, J.; Pakrasi, H. B. Use of Degradation Tags to Control Protein Levels in the Cyanobacterium Synechocystis Sp. Strain PCC 6803. Applied and Environmental Microbiology 2013, 79 (8), 2833–2835. https://doi.org/10.1128/AEM.03741-12.
- (35) Danino, T.; Mondragón-Palomino, O.; Tsimring, L.; Hasty, J. A Synchronized Quorum of Genetic Clocks. *Nature* **2010**, *463* (7279), 326–330. https://doi.org/10.1038/nature08753.
- (36) Gur, E.; Sauer, R. T. Evolution of the SsrA Degradation Tag in Mycoplasma: Specificity Switch to a Different Protease. *Proceedings of the National Academy of Sciences* 2008, 105 (42), 16113–16118. https://doi.org/10.1073/pnas.0808802105.
- (37) Baker, T. A.; Sauer, R. T. ClpXP, an ATP-Powered Unfolding and Protein-Degradation Machine. *Biochimica et Biophysica Acta - Molecular Cell Research* 2012, 1823 (1), 15–28. https://doi.org/10.1016/j.bbamcr.2011.06.007.
- (38) Hudson, C. M.; Williams, K. P. The TmRNA Website. *Nucleic Acids Research* 2015, 43 (D1), D138–D140. https://doi.org/10.1093/nar/gku1109.
- (39) Cameron, D. E.; Collins, J. J. Tunable Protein Degradation in Bacteria. *Nature Biotechnology* **2014**, *32* (12), 1276–1281. https://doi.org/10.1038/nbt.3053.
- (40) Chan, C. T. Y.; Lee, J. W.; Cameron, D. E.; Bashor, C. J.; Collins, J. J. "Deadman" and "Passcode" Microbial Kill Switches for Bacterial Containment. *Nature Chemical Biology* **2016**, *12* (2), 82–86. https://doi.org/10.1038/nchembio.1979.
- (41) Huang, D.; Holtz, W. J.; Maharbiz, M. M. A Genetic Bistable Switch Utilizing Nonlinear Protein Degradation. *Journal of Biological Engineering* 2012, 6, 1–13. https://doi.org/10.1186/1754-1611-6-9.
- (42) Chen, Y.; Kim, J. K.; Hirning, A. J.; Josić, K.; Bennett, M. R. Emergent Genetic Oscillations in a Synthetic Microbial Consortium. *Science* 2015, 349 (6251), 986–989. https://doi.org/10.1126/science.aaa3794.
- (43) Danino, T.; Mondragón-Palomino, O.; Tsimring, L.; Hasty, J. A Synchronized Quorum of Genetic Clocks. *Nature* **2010**, *463* (7279), 326–330. https://doi.org/10.1038/nature08753.
- (44) Liu, D.; Johnson, V. M.; Pakrasi, H. B. A Reversibly Induced CRISPRi System Targeting Photosystem II in the Cyanobacterium Synechocystis Sp. PCC 6803. ACS Synthetic Biology 2020, 9 (6), 1441–1449. https://doi.org/10.1021/acssynbio.0c00106.

- (45) Gibson, D. G.; Young, L.; Chuang, R. Y.; Venter, J. C.; Hutchison, C. A.; Smith, H. O. Enzymatic Assembly of DNA Molecules up to Several Hundred Kilobases. *Nature Methods* 2009, 6 (5), 343–345. https://doi.org/10.1038/nmeth.1318.
- (46) Clerico, E. M.; Ditty, J. L.; Golden, S. S. Specialized Techniques for Site-Directed Mutagenesis in Cyanobacteria. In *Methods in Molecular Biology, vol. 362: Circadian Rhythms: Methods and Protocols*; 2007; Vol. 362, pp 155–171.
- (47) Ausubel, F. M.; Brent, R.; Kingston, R. E.; Moore, D. D.; Seidman, J. G.; Smith, J. a; Struhl, K.; Wiley, C. J.; Allison, R. D.; Bittner, M.; Blackshaw, S. Current Protocols in Molecular Biology; 2003; Vol. 1. https://doi.org/10.1002/mrd.1080010210.
- (48) Chung, C. T.; Niemela, S. L.; Miller, R. H. One-Step Preparation of Competent Escherichia Coli: Transformation and Storage of Bacterial Cells in the Same Solution. *Proceedings of the National Academy of Sciences of the United States of America* 1989, 86 (7), 2172–2175. https://doi.org/10.1073/pnas.86.7.2172.
- (49) Chung, C. T.; Miller, R. H. Preparation and Storage of Competent Escherichia Coli Cells. Methods in Enzymology 1993, 218 (C), 621–627. https://doi.org/10.1016/0076-6879(93)18045-E.
- (50) Golden, S. S.; Sherman, L. A. Optimal Conditions for Genetic Transformation of the Cyanobacterium Anacystis Nidulans R2. *Journal of Bacteriology* **1984**, *158* (1), 36–42. https://doi.org/10.1038/pj.2014.11.
- (51) Golden, S. S.; Brusslan, J.; Haselkorn, R. Genetic Engineering of the Cyanobacterial Chromosome. *Methods in Enzymology* 1987, 153 (C), 215–231. https://doi.org/10.1016/0076-6879(87)53055-5.
- (52) Nakahira, Y.; Ogawa, A.; Asano, H.; Oyama, T.; Tozawa, Y. Theophylline-Dependent Riboswitch as a Novel Genetic Tool for Strict Regulation of Protein Expression in Cyanobacterium Synechococcus Elongatus PCC 7942. *Plant and Cell Physiology* 2013, 54 (10), 1724–1735. https://doi.org/10.1093/pcp/pct115.
- (53) Shaner, N. C.; Lambert, G. G.; Chammas, A.; Ni, Y.; Cranfill, P. J.; Baird, M. A.; Sell, B. R.; Allen, J. R.; Day, R. N.; Israelsson, M.; Davidson, M. W.; Wang, J. A Bright Monomeric Green Fluorescent Protein Derived from Branchiostoma Lanceolatum. *Nature Methods* 2013, 10 (5), 407–409. https://doi.org/10.1038/nmeth.2413.
- (54) Niederholtmeyer, H.; Wolfstädter, B. T.; Savage, D. F.; Silver, P. A.; Way, J. C. Engineering Cyanobacteria to Synthesize and Export Hydrophilic Products. *Applied and Environmental Microbiology* 2010, 76 (11), 3462–3466. https://doi.org/10.1128/AEM.00202-10.
- (55) Santos-Merino, M.; Torrado, A.; Davis, G. A.; Röttig, A.; Bibby, T. S.; Kramer, D. M.; Ducat,D. C. Improved Photosynthetic Capacity and Photosystem I Oxidation via Heterologous

- Metabolism Engineering in Cyanobacteria. **2021**, *118*, 2021523118. https://doi.org/10.1073/pnas.2021523118/-/DCSupplemental.
- (56) Jordan, A.; Chandler, J.; MacCready, J. S.; Huang, J.; Osteryoung, K. W.; Ducat, D. C. Engineering Cyanobacterial Cell Morphology for Enhanced Recovery and Processing of Biomass. *Applied and Environmental Microbiology* 2017, 83 (9), 1–13. https://doi.org/10.1128/aem.00053-17.
- (57) Ma, A. T.; Schmidt, C. M.; Golden, J. W. Regulation of Gene Expression in Diverse Cyanobacterial Species by Using Theophylline-Responsive Riboswitches. *Appl Environ Microbiol* 2014, 80 (21), 6704–6713. https://doi.org/10.1128/AEM.01697-14.
- (58) Gur, E.; Sauer, R. T. Recognition of Misfolded Proteins by Lon, a AAA+ Protease. *Genes and Development* **2008**, 22 (16), 2267–2277. https://doi.org/10.1101/gad.1670908.
- (59) Zheng, L.; Baumann, U.; Reymond, J. L. An Efficient One-Step Site-Directed and Site-Saturation Mutagenesis Protocol. *Nucleic acids research* 2004, 32 (14). https://doi.org/10.1093/nar/gnh110.
- (60) Rueden, C. T.; Schindelin, J.; Hiner, M. C.; DeZonia, B. E.; Walter, A. E.; Arena, E. T.; Eliceiri, K. W. ImageJ2: ImageJ for the next Generation of Scientific Image Data. *BMC Bioinformatics* 2017, 18 (1), 1–26. https://doi.org/10.1186/s12859-017-1934-z.
- (61) Schindelin, J.; Arganda-Carreras, I.; Frise, E.; Kaynig, V.; Longair, M.; Pietzsch, T.; Preibisch, S.; Rueden, C.; Saalfeld, S.; Schmid, B.; Tinevez, J. Y.; White, D. J.; Hartenstein, V.; Eliceiri, K.; Tomancak, P.; Cardona, A. Fiji: An Open-Source Platform for Biological-Image Analysis. *Nature Methods* 2012, 9 (7), 676–682. https://doi.org/10.1038/nmeth.2019.
- (62) Ronneberger, O.; Fischer, P.; Brox, T. U-Net: Convolutional Networks for Biomedical Image Segmentation. Lecture Notes in Computer Science (including subseries Lecture Notes in Artificial Intelligence and Lecture Notes in Bioinformatics) 2015, 9351, 234–241. https://doi.org/10.1007/978-3-319-24574-4_28.
- (63) Paszke, A.; Gross, S.; Massa, F.; Lerer, A.; Bradbury, J.; Chanan, G.; Killeen, T.; Lin, Z.; Gimelshein, N.; Antiga, L.; Desmaison, A.; Köpf, A.; Yang, E.; DeVito, Z.; Raison, M.; Tejani, A.; Chilamkurthy, S.; Steiner, B.; Fang, L.; Bai, J.; Chintala, S. PyTorch: An Imperative Style, High-Performance Deep Learning Library. In *NeurIPS*; 2019.
- (64) Bradley, L.; Sipőcz, B.; Robitaille, T.; Tollerud, E.; Vinícius, Z.; Deil, C.; Barbary, K.; Wilson, T. J.; Busko, I.; Donath, A.; Günther, H. M.; Cara, M.; Conseil, S.; Bostroem, A.; Droettboom, M.; Bray, E. M.; krachyon; Lim, P. L.; Bratholm, L. A.; Barentsen, G.; Craig, M.; Rathi, S.; Pascual, S.; Perren, G.; Georgiev, I. Y.; Val-Borro, M. de; Kerzendorf, W.; Bach, Y. P.; Quint, B.; Souchereau, H. Astropy/Photutils: 1.1.0. 2021. https://doi.org/10.5281/ZENODO.4624996.

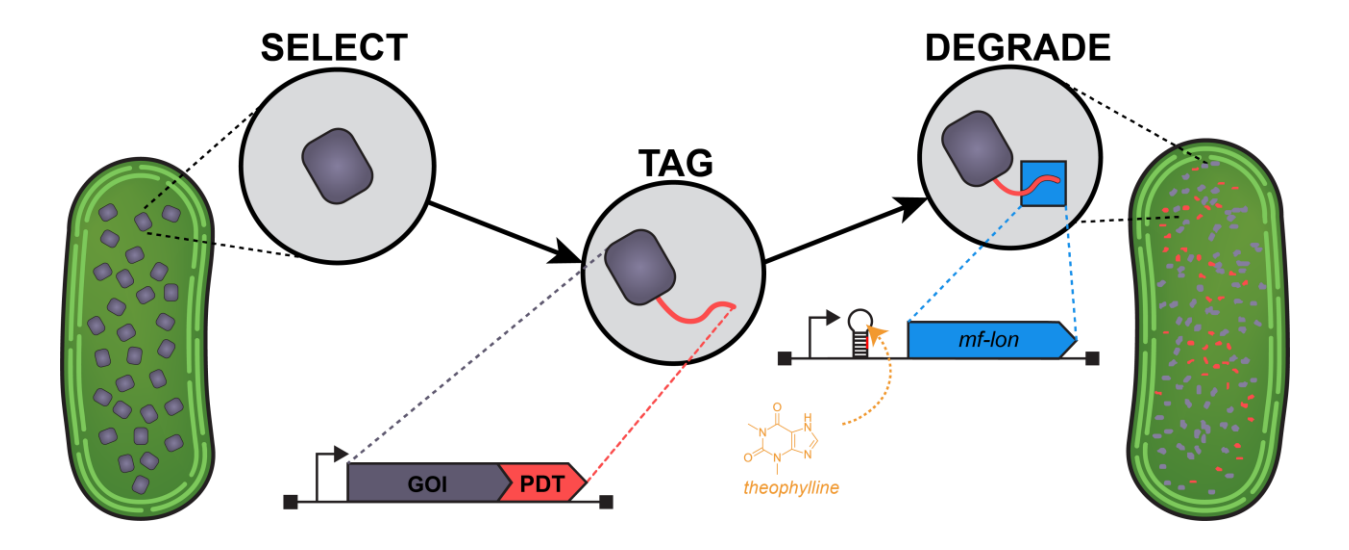
- (65) Maxwell, K.; Johnson, G. N. Chlorophyll Fluorescence A Practical Guide. *Journal of Experimental Botany* **2000**, *51* (345), 659–668. https://doi.org/10.1093/jxb/51.345.659.
- (66) Bindea, G.; Mlecnik, B.; Hackl, H.; Charoentong, P.; Tosolini, M.; Kirilovsky, A.; Fridman, W. H.; Pagès, F.; Trajanoski, Z.; Galon, J. ClueGO: A Cytoscape Plug-in to Decipher Functionally Grouped Gene Ontology and Pathway Annotation Networks. *Bioinformatics* 2009, 25 (8), 1091–1093. https://doi.org/10.1093/bioinformatics/btp101.
- (67) Mlecnik, B.; Galon, J.; Bindea, G. Automated Exploration of Gene Ontology Term and Pathway Networks with ClueGO-REST. *Bioinformatics* 2019, 35 (19), 3864–3866. https://doi.org/10.1093/bioinformatics/btz163.
- (68) Shannon, P.; Markiel, A.; Ozier, O.; Baliga, N. S.; Wang, J. T.; Ramage, D.; Amin, N.; Schwikowski, B.; Ideker, T. Cytoscape: A Software Environment for Integrated Models of Biomolecular Interaction Networks. *Genome Research* 2003, 13 (11), 2498–2504. https://doi.org/10.1101/gr.1239303.
- (69) Margolin, W. FtsZ and the Division of Prokaryotic Cells and Organelles. *Nature Reviews Molecular Cell Biology* **2005**, *6* (11), 862–871. https://doi.org/10.1038/nrm1745.
- (70) Mcquillen, R.; Xiao, J. Insights into the Structure, Function, and Dynamics of the Bacterial Cytokinetic FtsZ-Ring. **2020**. https://doi.org/10.1146/annurev-biophys-121219.
- (71) Du, S.; Lutkenhaus, J. At the Heart of Bacterial Cytokinesis: The Z Ring. *Trends in Microbiology*. Elsevier Ltd September 1, 2019, pp 781–791. https://doi.org/10.1016/j.tim.2019.04.011.
- (72) Miyagishima, S. Y.; Wolk, P. P.; Osteryoung, K. W. Identification of Cyanobacterial Cell Division Genes by Comparative and Mutational Analyses. *Molecular Microbiology* 2005, 56 (1), 126–143. https://doi.org/10.1111/j.1365-2958.2005.04548.x.
- (73) Addinall, S. G.; Bi, E.; Lutkenhaus, J. *FtsZ Ring Formation in Fts Mutants Downloaded From*; 1996; Vol. 178.
- (74) Gur, E.; Sauer, R. T. Degrons in Protein Substrates Program the Speed and Operating Efficiency of the AAA+ Lon Proteolytic Machine. *Proceedings of the National Academy of Sciences of the United States of America* 2009, 106 (44), 18503–18508. https://doi.org/10.1073/pnas.0910392106.
- (75) Wehrens, M.; Ershov, D.; Rozendaal, R.; Walker, N.; Schultz, D.; Kishony, R.; Levin, P. A.; Tans, S. J. Size Laws and Division Ring Dynamics in Filamentous Escherichia Coli Cells. *Current Biology* 2018, 28 (6), 972-979.e5. https://doi.org/10.1016/j.cub.2018.02.006.
- (76) Kerfeld, C. A.; Aussignargues, C.; Zarzycki, J.; Cai, F.; Sutter, M. Bacterial Microcompartments. *Nature Reviews Microbiology* 2018, 16 (5), 277. https://doi.org/10.1038/nrmicro.2018.10.

- (77) Kerfeld, C. A.; Melnicki, M. R. Assembly, Function and Evolution of Cyanobacterial Carboxysomes. *Current Opinion in Plant Biology* 2016, 31, 66–75. https://doi.org/10.1016/j.pbi.2016.03.009.
- (78) Sutter, M.; Laughlin, T. G.; Sloan, N. B.; Serwas, D.; Davies, K. M.; Kerfeld, C. A. Structure of a Synthetic β-Carboxysome Shell. *Plant Physiology* 2019, 181 (3), 1050–1058. https://doi.org/10.1104/pp.19.00885.
- (79) Marco, E.; Martinez, I.; Ronen-Tarazi, M.; Orus, M. I.; Kaplan, A. Inactivation of CcmO in Synechococcus Sp. Strain PCC 7942 Results in a Mutant Requiring High Levels of CO2. Applied and Environmental Microbiology 1994, 60 (3), 1018–1020.
- (80) Rae, B. D.; Long, B. M.; Badger, M. R.; Price, G. D. Structural Determinants of the Outer Shell of β-Carboxysomes in Synechococcus Elongatus PCC 7942: Roles for CcmK2, K3-K4, CcmO, and CcmL. PLoS ONE 2012, 7 (8), 14–19. https://doi.org/10.1371/journal.pone.0043871.
- (81) MacCready, J. S.; Hakim, P.; Young, E. J.; Hu, L.; Liu, J.; Osteryoung, K. W.; Vecchiarelli, A. G.; Ducat, D. C. Protein Gradients on the Nucleoid Position the Carbon-Fixing Organelles of Cyanobacteria. *eLife* 2018, 7, 334813. https://doi.org/10.7554/elife.39723.
- (82) Al-Haj, L.; Lui, Y.; Abed, R.; Gomaa, M.; Purton, S. Cyanobacteria as Chassis for Industrial Biotechnology: Progress and Prospects. *Life* 2016, 6 (4), 42. https://doi.org/10.3390/life6040042.
- (83) Ducat, D. C.; Way, J. C.; Silver, P. A. Engineering Cyanobacteria to Generate High-Value Products. *Trends in Biotechnology* 2011, 29 (2), 95–103. https://doi.org/10.1016/j.tibtech.2010.12.003.
- (84) Campbell, D.; Hurry, V.; Clarke, A. K.; Gustafsson, P.; Quist, G. O. ". *Chlorophyll Fluorescence Analysis of Cyanobacterial Photosynthesis and Acclimation*; 1998; Vol. 62.
- (85) Seidel, M.; Wickner, S. H.; Levchenko, I.; Flynn, J. M.; Baker, T. A.; Sauer, R. T. Overlapping Recognition Determinants within the SsrA Degradation Tag Allow Modulation of Proteolysis. *Proceedings of the National Academy of Sciences* 2002, 98 (19), 10584– 10589. https://doi.org/10.1073/pnas.191375298.
- (86) Lv, L.; Wu, Y.; Zhao, G.; Qi, H. Improvement in the Orthogonal Protein Degradation in Escherichia Coli by Truncated Mf-SsrA Tag. *Transactions of Tianjin University* 2019, 25 (4), 357–363. https://doi.org/10.1007/s12209-019-00193-z.
- (87) Bradley, R. W.; Buck, M.; Wang, B. Tools and Principles for Microbial Gene Circuit Engineering. *Journal of Molecular Biology* **2016**, *428* (5), 862–888. https://doi.org/10.1016/j.jmb.2015.10.004.
- (88) Mutalik, V. K.; Guimaraes, J. C.; Cambray, G.; Lam, C.; Christoffersen, M. J.; Mai, Q. A.; Tran, A. B.; Paull, M.; Keasling, J. D.; Arkin, A. P.; Endy, D. Precise and Reliable Gene

- Expression via Standard Transcription and Translation Initiation Elements. *Nature Methods* **2013**, *10* (4), 354–360. https://doi.org/10.1038/nmeth.2404.
- (89) Piechura, J. R.; Amarnath, K.; O'Shea, E. K. Natural Changes in Light Interact with Circadian Regulation at Promoters to Control Gene Expression in Cyanobacteria. *eLife* 2017, 6, 1–33. https://doi.org/10.7554/eLife.32032.
- (90) Mazouni, K.; Domain, F.; Cassier-Chauvat, C.; Chauvat, F. Molecular Analysis of the Key Cytokinetic Components of Cyanobacteria: FtsZ, ZipN and MinCDE. *Molecular Microbiology* 2004, 52 (4), 1145–1158. https://doi.org/10.1111/j.1365-2958.2004.04042.x.
- (91) Rueda, S.; Vicente, M.; Mingorance, J. Concentration and Assembly of the Division Ring Proteins FtsZ, FtsA, and ZipA during the Escherichia Coli Cell Cycle. *Journal of Bacteriology* **2003**, *185* (11), 3344–3351. https://doi.org/10.1128/JB.185.11.3344-3351.2003.
- (92) Sekar, K.; Rusconi, R.; Sauls, J. T.; Fuhrer, T.; Noor, E.; Nguyen, J.; Fernandez, V. I.; Buffing, M. F.; Berney, M.; Jun, S.; Stocker, R.; Sauer, U. Synthesis and Degradation of FtsZ Quantitatively Predict the First Cell Division in Starved Bacteria. *Molecular Systems Biology* **2018**, *14* (11), 1–14. https://doi.org/10.15252/msb.20188623.
- (93) Wang, N.; Bian, L.; Ma, X.; Meng, Y.; Chen, C. S.; Ur Rahman, M.; Zhang, T.; Li, Z.; Wang, P.; Chen, Y. Assembly Properties of the Bacterial Tubulin Homolog FtsZ from the Cyanobacterium Synechocystis Sp. PCC 6803. *Journal of Biological Chemistry* 2019, 294 (44), 16309–16319. https://doi.org/10.1074/jbc.RA119.009621.
- (94) Zhang, M.; Qiao, C.; Luan, G.; Luo, Q. Systematic Identification of Target Genes for Cellular Morphology Engineering in Synechococcus Elongatus PCC7942 Screening the Potential Genes Involved. 2020, 11 (July), 1–13. https://doi.org/10.3389/fmicb.2020.01608.
- (95) Taton, A.; Ma, A. T.; Ota, M.; Golden, S. S.; Golden, J. W. NOT Gate Genetic Circuits to Control Gene Expression in Cyanobacteria. ACS Synthetic Biology 2017, 6 (12), 2175– 2182. https://doi.org/10.1021/acssynbio.7b00203.
- (96) Wang, B.; Kitney, R. I.; Joly, N.; Buck, M. Engineering Modular and Orthogonal Genetic Logic Gates for Robust Digital-like Synthetic Biology. *Nature Communications* 2011, 2 (1). https://doi.org/10.1038/ncomms1516.
- (97) Wang, H.; Yan, X.; Aigner, H.; Bracher, A.; Nguyen, N. D.; Hee, W. Y.; Long, B. M.; Price, G. D.; Hartl, F. U.; Hayer-Hartl, M. Rubisco Condensate Formation by CcmM in β-Carboxysome Biogenesis. *Nature* 2019, 35. https://doi.org/10.1038/s41586-019-0880-5.
- (98) Ryan, P.; Forrester, T. J. B.; Wroblewski, C.; Kenney, T. M. G.; Kitova, E. N.; Klassen, J. S.; Kimber, M. S. The Small RbcS-like Domains of the -Carboxysome Structural Protein CcmM Bind RubisCO at a Site Distinct from That Binding the RbcS Subunit. *Journal of Biological Chemistry* 2019, 294 (8), 2593–2603. https://doi.org/10.1074/jbc.RA118.006330.

- (99) Rotskoff, G. M.; Geissler, P. L. Robust Nonequilibrium Pathways to Microcompartment Assembly. *Proceedings of the National Academy of Sciences of the United States of America* **2018**, *115* (25), 6341–6346. https://doi.org/10.1073/pnas.1802499115.
- (100) Sutter, M.; Greber, B.; Aussignargues, C.; Kerfeld, C. A. Assembly Principles and Structure of a 6.5-MDa Bacterial Microcompartment Shell. 2017. https://doi.org/10.1126/science.aan3289.
- (101) Hill, N. C.; Tay, J. W.; Altus, S.; Bortz, D. M.; Cameron, J. C. Life Cycle of a Cyanobacterial Carboxysome. *Science Advances* **2020**, 1–9. https://doi.org/10.1126/sciadv.aba1269.
- (102) Ducat, D. C.; Avelar-Rivas, J. A.; Way, J. C.; Silvera, P. A. Rerouting Carbon Flux to Enhance Photosynthetic Productivity. *Applied and Environmental Microbiology* **2012**, 78 (8), 2660–2668. https://doi.org/10.1128/AEM.07901-11.
- (103) Gupta, A.; Reizman, I. M. B.; Reisch, C. R.; Prather, K. L. J. Dynamic Regulation of Metabolic Flux in Engineered Bacteria Using a Pathway-Independent Quorum-Sensing Circuit. *Nature Biotechnology* 2017, 35 (3), 273–279. https://doi.org/10.1038/nbt.3796.
- (104) Niederholtmeyer, H.; Wolfstädter, B. T.; Savage, D. F.; Silver, P. A.; Way, J. C. Engineering Cyanobacteria to Synthesize and Export Hydrophilic Products. *Applied and Environmental Microbiology* 2010, 76 (11), 3462–3466. https://doi.org/10.1128/AEM.00202-10.

FOR TABLE OF CONTENTS USE ONLY



Title: Orthogonal degron system for controlled protein degradation in cyanobacteria

Authors: Jonathan K. Sakkos, Sergio Hernandez-Ortiz, Katherine W. Osteryoung, Daniel C. Ducat

Caption: Overview of the tunable degradation system from *M. florum*. The coding sequence for a gene of interest (GOI) in *S. elongatus* is appended with a 84 bp (26 AA) protein degradation tag (PDT). Upon induction of mf-lon protease with theophylline, the PDT is recognized by mf-lon and the protein is degraded.